Integrated Coastal Mapping of Dublin Bay Geomorphology based on geophysical data, satellite inferred bathymetry and 3D integration with INFOMAR datasets

Report: INF-11-07-GIB

Gibson, P. J., Martin-Himenes, D. and Caloca Casada, S.

2012

Summary

Geomorphological mapping and 3D geophysical characterization in County Dublin (Bull Island and Killiney Beach) allowed a depiction of the main stratigraphic and hydrostratigraphic units of two study areas, one encompassing coastal sedimentary processes and the other undergoing erosional processes. ERT data allowed the depth to bedrock in both areas to be estimated and and delineation of the spatial distribution of soft sediments in Killiney and the hydrostratigraphic units in Bull Island. These data provide extra information for future remedial actions related with sea level change potentially taken on urban areas. GPR data proved to be an excellent tool for depicting the internal architecture of sand dune deposits, the display of the data as 2.5D fence diagrams improved the knowledge on the genesis and evolution of the island. However, this method performed quite poorly in the Killiney study site. The lithological composition of the sediments with high silt and clay content did not allow for deep penetration of the electromagnetic waves. Seven different radar facies are recognized on the basis of reflection character and geometry in Bull Island. Most of the dunes are composed of foreslope and rearslope accretion deposits, the slacks between slopes are either composed of interstratified foreslope and rear-slope deposits and/or bio-topographic accumulation deposits. Foreslope deposits are characterized by moderately continuous subparallel gently seaward dipping reflectors, some of these present a continuous reflector dipping southeast showing continuity under the water table illustrating the former coastline. Rearslope accretion deposits are defined by discontinuous sinuous oblique reflectors and bio-topographic accumulation is illustrated by low amplitude discontinuous sinuous concave and convex-up reflectors. Embryonic dunes are recorded along the seaward side of the foredunes system for 2.5 Km from Dublin Port North Wall and are characterized by high amplitude continuous reflector combined with scattered oblique chaotic reflectors. Large freshwater marshes are characterized by high amplitude continuous horizontal reflectors. Salt marsh is also defined by high amplitude continuous horizontal reflectors. Marine sediments consisting of continuous seaward gently dipping moderately continuous reflectors mostly developing beneath the water-table underlain all the deposits described. Finally, man-made ground consisting of dams built to protect the fresh water marshes and golf links from seawater flooding are characterized by chaotic reflectors.

Table of Contents

1. Introduction

Soft, low-lying shorelines of Co. Dublin are highly exposed and vulnerable to negative impacts of climate change, of which sea-level rise is the most widespread consequence. A change in mean sea level will be enhanced by any increase in wave energy, surge levels, storm frequency and severity (IPCC, 2007).Evidence of changes in the Dublin coastline since the nineteenth century have been previously inferred from secondary sources, including historical maps, charts, documents and aerial photographic surveys (Mulrennan,1990; 1993) in the low-lying, dune-covered sand spit of Bull Island and also on the sand, gravelly beaches and unconsolidated cliffs of Killiney Beach-Bray by Robinson (2009). Coastal geomorphology and continuous offshore–onshore high resolution bathymetric data together with tide gauge data linked with remote sensing information from satellite imagery are two essential indicators for coastal vulnerability assessment studies to predict possible effects of climate change and sea level rise on the coastline (Mclaughlin, S. 2001; Thieler et al., 2000; Pendleton et al., 2010; McFadden et al,. 2007). Coastal morphological development is a physical expression of how energy is being mitigated. The stability of the foreshore shows evidence of major changes in wave penetration, storm magnitude and frequency and also is indicative of sediment exposure to erosion. Dune shape and movement and coastal vegetation are potentially sensitive to physical hazards related to climate change and sea level rise. In this area, geophysical data will help to establish a ranking of the coastal geomorphology regarding the susceptibility of different sedimentary structures/types to change prior to development/mitigation in the future (Robinson, 2009). Bathymetry and subtidal substrate slope of the near shore zone strongly influence the wave activity and exposure of the coastline and therefore the physical response of sandy barriers to sea-level rise (Sharples, 2006). As a consequence, a continuous offshore–onshore high resolution topography in the Dublin coastal area derived from terrestrial LIDAR and new bathymetry datasets will be essential for assessing the risk of inundation and shoreline retreat and will provide information on wave energy dissipative gradients and potential storm surge heights.

The first, and main aim of the project is to map the coastal geomorphology and the subsurface internal architecture of two study areas in Co. Dublin (see Figure 1.1) using Ground Penetrating Radar (GPR) and Electrical Resistivity Tomography (ERT). The final product will be an integrated 3D reconstruction of the coastal-near offshore

geomorphology showing the internal structure of the area based on field mapping and pre-existing datasets. Secondly, the methodology to produce a high resolution bathymetric map derived from satellite imagery of coastal Irish waters will be determined. This dataset would add to and complement greatly the current incomplete coastal topography from the Dublin Bay area derived from multi-beam bathymetry acquired by the INFOMAR Project (2010) and LiDAR digital terrestrial elevation model created from the Office of Public Works (2006) and the Ordnance Survey of Ireland (2009).

Figure 1.1 - Study sites: Bull Island (north) and Killiney (south).

This work was undertaken May-September 2012. Data were collected by Paul Gibson and Diego Martin-Jimenez of the Environmental Geophysics Unit of the Department of Geography, National University of Maynooth and by Silvia Caloca Casada of ICARUS, Department of Geography, National University of Maynooth.

The geophysical survey data will enable the internal characteristics of the subsurface to be determined. These datasets will, in the future, aid in the construction of erosion and storm flooding models. Geophysical results will also be correlated with relevant indicators of coastal change such as depth to bedrock profiles and available historical erosion rates, in order to elucidate which sedimentary structures/types are more likely to contribute to change and to understand the conditioning factors. Geophysical data will also be used to estimate the depth to the water table. SPOT satellite imagery will also be employed to determine zones of change at the sites to help in the geophysical traverse locations.

1.1. Geographical and Geological Setting

County Dublin is largely covered by soft sediments (till, sand and gravel, lacustrine, alluvial and marine sediments), bedrock, underlying these sediments, mainly outcrops in areas of North Co. Dublin, Howth Peninsula and Wicklow Mountains. Cambrian age bedrock consisting of a melange of quartzite blocks with mudstone to siltstone matrix, greywacke, siltstone, mudstone and calcareous sandstone are recorded in Howth Peninsula. Granite dominate the hills of Killiney and Dalkey and the Central parts of the Wicklow mountains. Ordovician slates, phyllites and schists with inlying Cambrian greywackes and quartzite underlie the Killiney beach area (McConnell et al., 1994). Lower Carboniferous limestone and shale dominate the lower ground areas, the Lucan Formation is the most extensive bedrock type; it underlies most of Dublin City and consists of laminated argillaceous calcisiltites and calcareous shales. Lower Carboniferous rocks are delimited by a fault contact to the south with the Lower Palaeozoic Rocks and the Leinster Granite batholith and by Lower Palaeozoic Rocks to the north (McConnell et al., 1994).

The current profile of the County Dublin coast was mainly shaped during the last (MIS 2) glaciation between ca. 26 ka and ca. 17.3 ka BP (Ballantyne et al., 2006). Three ice

sheets/domes interacted in the area during the last glaciation. The Irish Sea Ice Sheet, with its accumulation area located in the Scotland highlands, advanced southwards by the Irish Sea depression (Synge, 1977). This ice stream coalesced in the Dublin area with the Northern Ice Dome with its centre of mass located in the northern Irish Midlands flowing south-eastwards and with the Wicklow Mountains Ice Sheet which was flowing northwards within County Dublin (Hoare, 1975). These ice masses released large amounts of glacial and glaciofluvial sediments during ice retreat. This is illustrated by mean minimum average Quaternary sediments thickness in County Dublin of over 4.5 m reaching maximums of over 30 m in the areas of Dublin Port and Killiney beach (Pellicer, 2008).

The most common deposits in the County Dublin are glacial and glaciofluvial sediments derived from Lower Carboniferous limestone bedrock. The north County Dublin uplands area is mainly covered by diamictons and glaciofluvial sediments derived from Lower Palaeozoic sandstone and shale, volcanic rocks and Namurian sandstone and shale. The lowland Dublin City area is dominated by diamicton derived from Lower Carbonifereous Limestone, classified on two main members: brown and black boulder Clay, where the brown boulder Clay has been interpreted as a weathered layer of the black boulder Clay (Farrell et al., 1995), other soft sediments are glaciofluvial sands and gravels, marine sediments and Aeolian sediments in the coastal areas andfill deposits on the Dublin Port area. The south Dublin Mountains are dominated by diamicton and glaciofluvial sediments derived from Lower Palaeozoic sandstone and shale, metamorphic and granite bedrock, with small patches of Limestone derived sediments. Evidence from erratic distribution indicates that Irish Sea Ice Sheet penetrated onshore for at least 20 Km in the Dublin lowlands area. On the other hand, geomorphological glacial features (i.e. meltwater channels, ice marginal ridges and drumlins) illustrate main ice withdrawal directionof the Midland and Wicklow ice domes (Pellicer, 2008). Postglacial sediments are represented by lacustrine silts and clays, peat, alluvial clays, silts, sands and gravel and marine deposits.

The coastal systems in this region can be divided in two main morphological types, flat coast (or graded shoreline) constituted of sandy and gravelly beaches, tombolos, sand and gravel spits and barriers with associated lagoons, dunes salt marshes and wetlands and cliffed or abrasion coast composed of either hard rock cliffs and soft sediments

cliffs (Carter, 1991). Hard rock cliffs are morphologically expressed as headlands, whereas soft sediment cliffs, undergoing intensive erosion processes, show a bay-like coastal profile. Main geomorphological coastal features in County Dublin are presented from north to south: (i) A series of barrier-beach complexes developing at the mouth of estuaries lying between resistant headlands are described along the north County Dublin coastline, these barriers formed as sea levels rose during the postglacial Holocene marine transgression. Unconsolidated glacial clays, sands and gravels were incorporated into coarse grained storm beach ridges, partly closing the bays and creating estuaries behind them (Mulrennan, 1990); (ii) the Howth Peninsula headland is connected to the mainland by a tombolo composed of sand, which formed during a sea-level rise episode about five thousand years ago (Harris, 1977); (iii) Dublin Bay, flanked by the Howth and Dalkey headlands is dominated by large sand banks at both margins of Dublin Port and culminated in Bull Island by a large sand dune complex; finally (iv) the Killiney/Bray beach mostly sheltered by a soft sediments cliff to the west is flanked by the Dalkey(to the north) and the Bray (to the south) headlands.

The study area is divided into two sites situated along the coastline of County Dublin, Bull Island to the north and Killiney beach/cliff to the south (Figure 1.1). Bull Island is a 5 Km long island, which formed during the last two centuries subsequent to the building of the Dublin Port North Wall. The island is banked against the Dublin Port North Wall to the south and bounded by Sutton Creek to the north, a marine channel feature running along the south of Howth Peninsula. Killiney beach situated north of Bray, consist of a over 6 Km long portion of soft coastline composed of a narrow gravelly beach and a continuous soft sediments cliff undergoing extensive erosion and flanked by the hard coast areas of Bray head to the south and Dalkey head to the north.

Bull Island

Bull Island is a wedge shaped narrow portion of land orientated southwest-northeast about 5 Km long, ranging in width between 1 Km at its southwest end and 200 m to the northeast (Figure 1.2). It encompasses mean altitudes of 2.8 m OD, reaching a maximum of just over 9 m OD in the central-northeast region. The island is connected to the mainland in two places, at the southwest end by a bridge linking the Dublin Port north wall to Clontarf and by a Causeway road at its central part constructed during the

1960s. It started to form after the building of the wall at the end of the 19th century as a narrow ribbon of sand and has been growing south-eastwards since. It can be divided by three main physiographic units distributed parallel to the coast: (i) a wide sandy beach with a nearly flat profile at the south-east margin of the island; (ii) a large sand dune area, wider to the southwest gradually narrowing north-eastwards partially disturbed by the development of two golf links at the south and mid regions of the island and; (iii) a flat salt marsh area at the northeast margin of the island encompassing average widths of 200 m. Bull Island has been divided into three sub-sites showing different geomorphological settings. Site 1 to the north region of the Island, Site 2 situated in the middle area, north and south of the causeway road connecting the island with the mainland, and Site 3 located by the Dublin Port North Wall (Figure 1.2).

Figure 1.2 – Location of Bull Island study site and sub-sites. BH: borehole data.

Killiney Beach

Killiney Beach is a long narrow gravelly beach over 6.5 Km long orientated south-north and sheltered to the west by a 5 to 16 m high cliff face (Figure 1.3). The north 2.5 Km of the beach is mainly composed of coarse gravel with some cobbles and boulders in

places, it consist of a generally steep beach encompassing mean beach widths of about 30 m, reaching a maximum of over 50 m in the area between the Shanganagh and Loughlinstown rivers. The southern half of the beach encompasses widths of less than 30 m, has a generally steep profile and is dominated by gravels, cobbles and boulders. The cliff located west from the beach shows continuity from Bray harbour to the Shanganagh River for 3 Km, it loses continuity for 500 m in the Loughlinstown River mouth area and emerges again to the north for 380 m as a soft sediment cliff passing into a hard rock cliff giving into the Dalkey headland.

Killiney beach has been divided in three sub-sites. Site 1 located in the Shanganagh River area to the north, Site 2 situated in a park located in the middle are were intensive coastal erosion is noticed along the cliff and Site 3 located north of Bray (Figure 1.3).

Figure 1.3 – Location of Killiney beach study site and sub-sites.

1.2. Pre-existing datasets

A number of datasets available allowed a pre-characterization of the geomorphology and sedimentology for the study area. Two Digital Elevation Models (DEMs) and several orthophoto datasets were used for characterizing the geomorphology of the study areas and, with SPOT imagery, to aid in the selection of the study sites. These were: the Office of Public Works DEM (2 m pixel size) and the orthophoto mosaic (0.25 m pixel size) for Bull Island from 2006; the DEM (10 m pixel size) and the orthophotos (1 m pixel size) from 2000 and the black and white orthophotos from 1995

produced by the Ordnance Survey of Ireland and supplied by the Geological Survey of Ireland (GSI). Furthermore, the GSI supplied bedrock and Quaternary geology maps for County Dublin in ArcGIS format and borehole records extracted from the geotechnical database (Figure 1.4), which permitted a broad characterization of the subsurface geology.

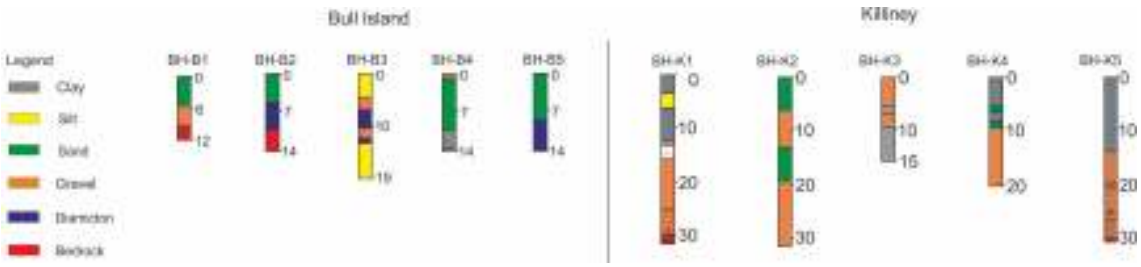

Figure 1.4 – Borehole records compiled from the Geological Survey of Ireland Geotechnical database for Bull Island and Killiney beach study areas.

2. Methodology

Two geophysical techniques were employed in this study:

- Electrical resistivity tomography (ERT)
- Ground penetrating radar (GPR).

The integration of electrical and electromagnetic geophysical techniques as complementary tools for unconsolidated sediments characterization has been widely explored during the last decade (e.g. Slater and Reeve, 2002; Comas et al., 2004; Vanneste et al., 2008, Doetsch et al., 2011).In Ireland, GPR surveys have proven to be very successful in differentiating between sediments and detecting subsurface discontinuities due to changes in lithology, the internal architecture and presence of the water table (Caloca, 2006; Trafford *et al*., 2009; Pellicer, 2010).

Resistivity theory

Resistivity is a characteristic that can be measured by geophysical means. The resistivity of pure refined metals is very low and they are in fact very good conductors. The resistivity of naturally occurring substances are many orders of magnitude greater than the resistivity of metals. There is often a substantial overlap between the resistivity of one substance and the resistivity of another, thus the resistivity value is not diagnostic of a specific substance. Most natural substances have a range of values which is substantially greater than the equivalent density range or susceptibility range for the same substance.

Electric current can be conducted by electrolytic conduction which requires the presence of a liquid. Pure water is not a good conductor but most natural water contains dissolved salts which facilitate current flow. The nature of the electrolyte controls the resistivity/conductivity. The resistivity of seawater which contains sodium and chloride ions is much lower than the resistivity of fresh water. The resistivity of a natural substance such as a rock layer or glacial moraine will consequently vary greatly depending on the amount of liquid and the type of liquid present. A rock layer will, all other things being equal, have a higher conductivity (lower resistivity) if it is permeated

by a saline solution rather than a fresh water solution. Even small amounts of water can dramatically alter the resistivity by many orders of magnitude.

Sedimentary rocks and unconsolidated sediments are composed of grains which allow the pores between the grains to be infilled with fluid. Igneous rocks such as granite although they are formed of interlocking crystals often contain cracks and joints which can contain water and result in a low resistivity. Similarly, metamorphic rocks can contain cracks which can contain liquids. Another complication that can occur with metamorphic rocks is that the resistivity of a particular volume of rock may be different if measured in different directions. This is because some metamorphic rocks such as slate or schist display a pronounced alignment of minerals and in general the resistivity is lower for measurements parallel to the alignment and higher at right angles to the alignment. Other factors may also affect the resistivity. As a sedimentary rock gets older the pore spaces may become infilled with deposits, expelling the interstitial fluids or the increased weight of sediments may cause compaction. A weathered rock or a highly porous permeable rock will tend to have a lower resistivity than an unweathered one or one which is non-porous or impermeable.

Resistivity surveying equipment

Resistivity surveying equipment has a number of simple components: a resistivity meter housing a source of current and a means to measure the voltage and wires connected to electrodes through which the current is injected into the ground. There are various types of resistivity meter (e.g. Tigre 32; IRIS Instruments SYSCAL system; ABEM TERRAMETER SAS 4000) thus details vary but they conform to a general pattern. The resistivity meter is housed in a lightweight waterproof shell, with the controls, display and connectors on the top panel. The standard type of meter has four connectors two for the two potential and two current electrodes. The operator has the option to pick the current setting from a number of preset values. A number of readings are obtained at one location and an average value obtained. The power output for most systems can be boosted using optional or external equipment which allows the delivery of larger currents. Typically, resistivity meters have power outputs of the order of 50 - 100W.

2D electrical imaging

Figure 2.1 - ERT survey

Two dimensional electrical imaging (also termed tomography) allows the acquisition of apparent resistivity variations in both the vertical and horizontal directions. It effectively produces a 2D slice which is known as a pseudosection. Electrical imaging is mainly undertaken using an insulated multi-core cable with a number of fixed interval take off points to which electrodes are connected. The length of the cable, number of take-off points and interval between them can vary. Typical cables use 32 – 64 electrodes with take-off points at fixed intervals. The cable is connected to the meter which in turn is connected to a laptop computer which determines which set of 4 electrodes are used in the measurements, Figure 2.1.

Repeating this procedure for higher levels allow the production of a pseudosection which displays the apparent resistivity variations in two dimensions. The depth at which the data are plotted is generally the median depth of investigation for the particular electrode array for that specific level.

Although the pseudosection provides some information about the subsurface it is important to remember that different pseudosections would be produced for the same

profile if different electrode arrays are used. The data must be modeled using a computer program in order to determine how the true resistivity varies with depth. One such program that is widely used in resistivity work is the inversion program RES2DINV. This program can be explained best by referring to Figure 2.2. The topmost image in this figure shows the variation in measured apparent resistivity for a 115m long line. The subsurface is divided into a number of blocks which are assigned resistivity values and an initial model of the surface is formed which shows the variation in true resistivity with real depth. The apparent resistivity that this model would yield for the electrode array that is used is then calculated and compared to the measured apparent resistivity. The model is then progressively altered using a least-squares optimization approach in order to reduce the Root Mean Square (RMS) error between the calculated and measured apparent resistivity. The center image in Figure 2.2 shows the calculated resistivity that the model (bottom image) would produce. In this instance it is clear that there is quite a good match between the calculated and measured apparent resistivities, thus the model can be assumed to be a good representation of the subsurface variation in true resistivity. It is possible to alter some of the programs parameters. This may result in some differences in the fine detail of the model but the gross variation would be similar.

A Wenner-Schlumberger array was used in this survey with 32 and 25 electrodes using a Tigre 32 Resistivity meter. Electrode spacing varied on different lines. 2m spacings were used to provide detail near the surface, 5m spacings provided information to depths of about 22m and 10m spacings (using 25 electrodes) were used to determine the depth to bedrock (45m penetration).Resistivity data was processed with RES2DINV and RES3DINV software packages. Fence diagrams and 3D resistivity volumes were produced and displayed with Voxler software.

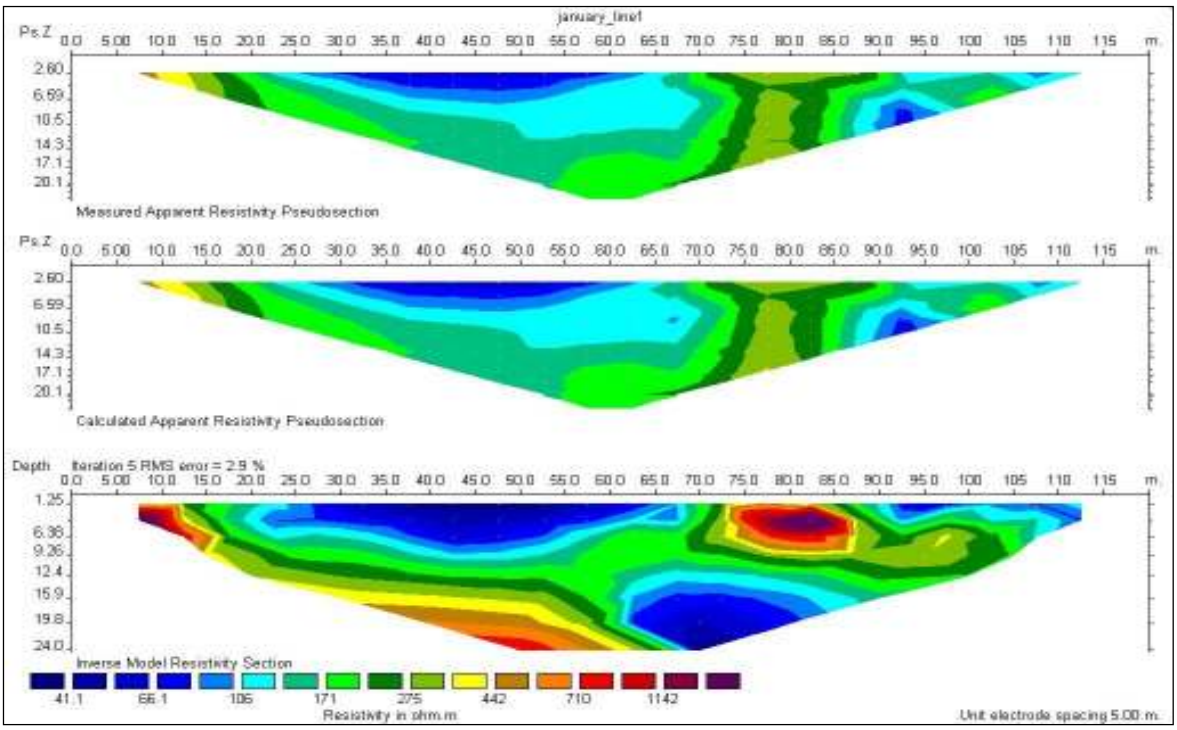

Figure 2.2 – RES2DINV produces an inverse resistivity model from the measured apparent resistivity pseudosection. A calculated apparent resistivity pseudosection is generated from the inverse model. The error obtained (2.9%) is the difference between the measured and the calculated pseudosections..

Ground Penetrating Radar

Ground penetrating radar (GPR) is an electromagnetic geophysical technique which can, under certain circumstances, provide a very detailed image of the subsurface. In essence, GPR consists of transmitting electromagnetic (EM) pulses into the ground and measuring the signals that are reflected back from subsurface interfaces or bodies and the times at which these signals are acquired at the receiver. GPR systems are designed to operate at different frequencies ranging from about 10 MHz to 1500 MHz.

The GPR data were collected with Geophysical Survey Systems, Inc (GSSI) system with 100MHz and 200MHz antennae (Figure 2.3). A high voltage electrical pulse, is sent from the console to the transmitter and the pulse is injected into the ground via the transmitter antenna which has a designated central operating frequency. As the input energy wave travels down in encounters discontinuities in the subsurface such as changes in rock type, water content or walls and some of the input energy is reflected

back towards the surface. The reflected signal is recorded by the receiver and the results are shown on a display unit which is the screen of a laptop computer. The data are stored digitally on the computer which also contains the software programs used to control the collection of the data and also the processing of the radar data.

The GPR system was used in constant offset mode. In constant offset mode, the receiver and transmitter antenna are kept a fixed distance apart. The system is set to collect readings at a predetermined distance and an odometer wheel is used to measure this distance. The two-antenna setup is dragged along the surface and the system automatically collects a reading at the predetermined distance. Distance between readings varies and depends on the frequency used and the size of the subsurface target.

a b

Figure 2.3– (a) 200 MHz and (b)100 MHz antennae GSSI GPR systems in operation.

A typical radar profile (sometimes referred to as a radargram) is composed of a number of traces which is a record of the reflections at one point. The number of traces will vary depending on the length of the traverse and how often data are recorded along the traverse. A 20 m long traverse will be composed of 201 traces, if data are obtained at 10 cm intervals. A sequence of closely spaced traces allows the continuity of reflectors to be examined. The horizontal axis shows the location along the traverse whereas the vertical axis gives the two-way transit time for the EM waves. Shallow features have shorter travel times than deeper features and consequently appear higher up in the section. The velocity of the EM waves in the subsurface must be known, estimated or measured in order to determine the true depth of features below the surface.

In order to undertake a successful GPR survey, there are a number of parameters which have to be decided on and which may need to be input into the computer program used when collecting the data. These include frequency, time window duration and temporal and spatial sampling intervals.

Frequency

GPR systems are designed to operate with antennae which transmit and receive at specific frequencies. The choice of operating frequency is crucial if a project's objectives are to be achieved as it strongly controls the depth of investigation and the resolution that is obtained. Skin depth (which is inversely proportional to attenuation) depends on the operating frequency. Decreasing frequency increases the skin depth and reduces the attenuation. Therefore the lower the operating frequency of a GPR system, the deeper the depth of investigation. However, the lower the frequency the poorer the vertical resolution of the system. Data were collected on all lines using an antennae frequency of 100 or 200 MHz.

Time window duration

The time window is the temporal interval during which reflected data are measured and saved. If the time window is very short then important reflection events at depth may not be recorded. However, setting too long a time window may be inefficient as attenuation may limit the depth of investigation to only a few meters. The time window is equal to twice the depth of investigation (as the radar wave has to travel down to the reflector and the reflected wave back up to the receiver) divided by the subsurface velocity. In general, the time window for lower frequency antennae tend to be greater than for higher frequency ones as the former have a greater depth of investigation. A time window of 150 ns was employed in the survey.

Temporal and spatial sampling intervals

The returned signals are regularly sampled and should not exceed half the period of the highest frequency signal. In this survey data was collected in continuous mode using an odometer, a distance of 5 cm was set to collect the data for both 100 and 200 MHz antennae, which is within the minimum distance between readings recomended in the literature for both 100 MHz and 200 MHz antennae (Jol and Bristow, 2003).

Post-processing of GPR data

Various computer programs are available to process radar data in order to maximise the amount of information that can be extracted. These programs allow the radar files to be edited e.g. datasets can be reversed, resampled or merged or they can be processed by applying gains, temporal or spatial filters. Preliminary data processing was performed with Radan software package. Data were then converted to PulseEkko format and processed using the software packages EkkoView and EkkoView deLuxe (Sensors and Software, 2001 and 2003). 3D GPR data was compiled using EkkoMapper, edited with GFP Edit and displayed with Voxler software.

GPR data processing encompassed the following steps: (i) radargram velocity calibration, the depth of all the datasets in Bull Island were corrected with a velocity of 0.11 m/ns and datasets in Killiney beach with a velocity of 0.1 m/ns, the correction was based on hyperbolae reflection analysis. (ii) automatic time zero adjustment; (iii) application of a high pass filter or dewow. Although the transmitted radar pulse is mainly at a high frequency, the low frequency component slowly decays and the reflections are superimposed on this decaying transient, GPR data are high pass filtered (dewowed) to suppress the low frequency component and to pass the antenna center frequency; (iv) application of a low pass filter; (v) topography correction, topography data were collected using a Trimble RTK GPS system and extracted from the DEM data available and; (vi) application of an Automatic Gain Control (AGC).

Datasets were subsequently edited using the radar facies methodology presented by Neal (2004) and fence diagrams and 3D volumes were produced and displayed using the Voxler software package.

3. Geomorphology and results based on geophysical data

Geomorphology

The study area is divided into two sites situated along the coastline of County Dublin, Bull Island to the north and Killiney beach/cliff to the south (Figure 1.1). Bull Island is a 5 Km long island, banked against the Dublin Port North Wall to the south and flanked by Howth head to the north. Killiney beach situated north of Bray, consist of a over 6 Km long portion of soft coastline composed of a narrow gravelly beach and a continuous soft sediments cliff undergoing extensive erosion and flanked by the hard coast areas of Bray head to the south and Dalkey head to the north.

3.1.1. Bull Island

Bull Island can be divided in four main geomorphological units: the beach complex situated along the southeast coastline, the sand dune complex covering the higher ground areas, the salt marsh along the northwest coastline and the sand/mud flat area covering the region between the island and the mainland, Figure 3.1.

The beach complex extends seawards alongthe southeast coastline for about 600 m in the southern region and reaches a maximum width of 900 m in the northeast of the island along Sutton Creek. It is composed of a series of ridges and runnels truncated in places by drainage channels running normal to them and gradually increasing in number towards the northeast parts of the island where the beach profile is less steep (Harris, 1977).

The sand dune complex located in the central part of the island extends for 5 Km from southwest to northeast, it consist ofa 840 m wide sand dune complex in the southwest region along the North Bull Wall and gradually thinning to the northeast where it tails off in a recurve constrained to the northeast by Sutton Creek. The southwest region of the dune complex is partly disturbed by the golf-links. Dune ridges with poor topographic expression develop in thisareain combination with large fresh water marsh areas. The ridges become gradually higher, parallel and better developed north-eastwards as the fresh water marsh areas become confined in the inter-dune areas gradually slacking off. Furthermore, a generally continuous ridge of embryonic dunes develop for about 2.5 Km from the Dublin Port North Wall, indicative of on-going accretion processes in this area. In the region covered by Site 2 (Figure 1.2) and north-eastwards from it the dune ridges lose some continuity and several blowouts are

recognized. North from Site 2 the dunes become larger, reaching maximum altitudes of 9 m OD. In this, area two diverging dunes which converge again to the northeast allowed for the development of a the Alder Marsh, a fresh water marsh of significant ecological value (Devaney, 2008). In the region to the northeast, where these sand dunes converge in a single dune ridge, an area showing circular dunes named Green Island is recognized. Green Island precedes the development of the longitudinal sand dune cordons dominating the north parts of Bull Island, its formation has been dated previous to 1869 (Harris, 1977), thus illustrating the palaeo-coastline more than 150 years ago. North of Green Island a single foredune ridge diverges out into several ridges forming the recurve at the northeast end of Bull Island.

Salt marsh deposits develop along Bull Island northwest coast between the dunes and the lagoon, a sharp change in slope corresponding to the high water limit delimits it from the lagoon area. It is composed of a mixture of sandy mud with plant remains and a series of drainage creeks meandering from the dunes to the lagoon (Harris, 1977). The lagoon area was divided by Harris (1977) into three separate regions: lagoonal mud flat covering the north margin of the Bull Island causeway; the salicornia mud flat, which spread largely subsequent to the construction of the causeway and; the lagoonal sand flat covering most of the lagoon in the areas strongly influenced by tidal currents.

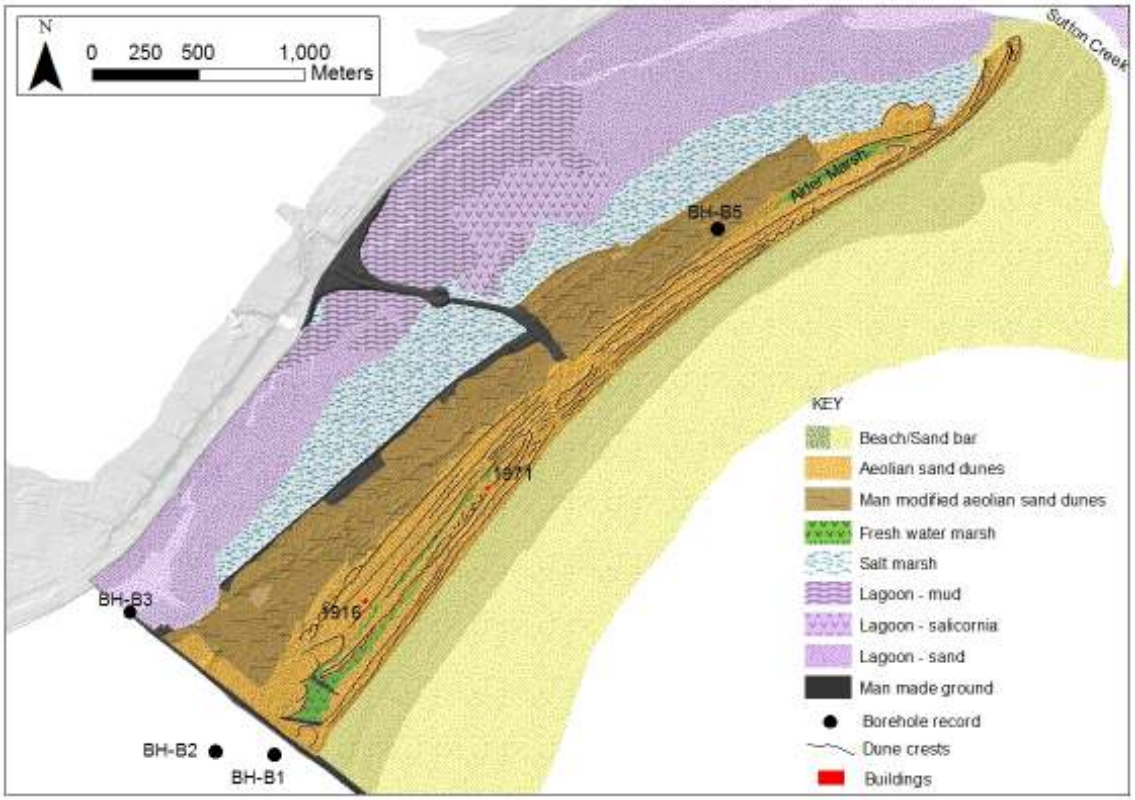

Figure 3.1 – Geomorphology and sediment distribution map for Bull Island, modified from Harris (1977). Sun illuminated DEM from OPW (2006) is used as topographic background.

3.1.2. Killiney Beach

Killiney Beach is a long narrow gravelly beach over 6.5 Km long orientated south-north and sheltered to the west by a 5 to 16 m high cliff face. The cliff face is composed of interstratified tills, sands and gravels which deposited during the last Fenitian glaciation (Warren, 1985). The cliffs delimit the eastern margin of a narrow coastal plain delimited by Bray head to the south, the granite hills of Killiney and Dalkey to the north and tills derived of limestone, metamorphic andgranite bedrock underlain by metamorphic rocks to the west (Figure 3.2). Numerous interpretations have been proposed for the deposition of the sediments constituting the coastal plain (Synge, 1963; Mitchell, 1972; Bowen, 1973; Eyles and McCabe 1989a,b; Warren, 1991; Rijsdijk et al., 2010). The latest work by Rijsdijk et al. (2010) proposes a terrestrial origin of these sediments. The sediments constituting the coastal plain deposited during the last glaciation and experienced widespread deformation through various episodes of ice advance and retreat. Rijsdijk et al. (2010) identified areas of compression and extension along the Killiney cliff associated with the deformation process, areas dominated by compression

extend from Killiney to the south of Site 1, while extension dominates the southern parts of the cliff from Site 2 to Bray. Geophysical surveys were carried out in compressional (Site 1) and extensional (Site 2) sections of the cliff. Furthermore, the coastal plain has undergone continuous erosion since deposition, the railway line connecting Dublin and Bray wasshifted westwards at the beginning of the last century due to the rapid coastal erosion in the area, coastal erosion along the Killiney beach cliff has been estimated on ca. 25 m during the last 100 years (Rijsdijk et al., 2010).

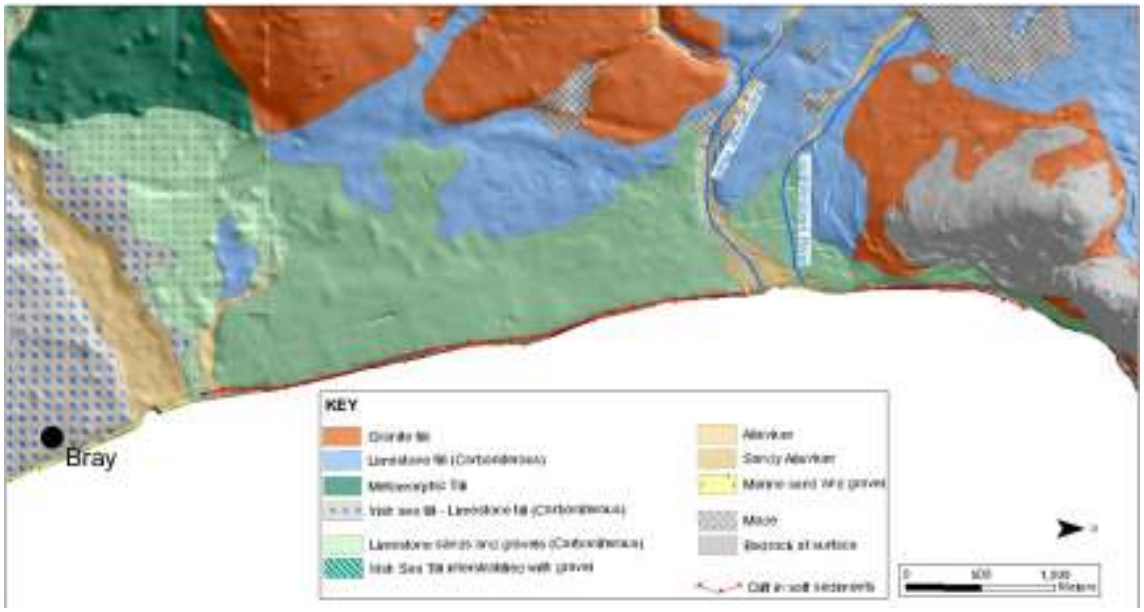

Figure 3.2 – Sediment distribution map for Killiney beach area, modified from Geological Survey of Ireland Quaternary Geology map.

3.2. Geophysical Surveys

3.2.1. Bull Island

3.2.1.1.Resistivity

Bull Island - Site 1

A total of seven lines were recorded in Site 1 of Bull Island which are presented and described below. Four lines were collected using an electrode spacing of 5m, one with 10 m and two with 2 m (Figure 3.3). These data allow a broad characterization of the existing lithological types.

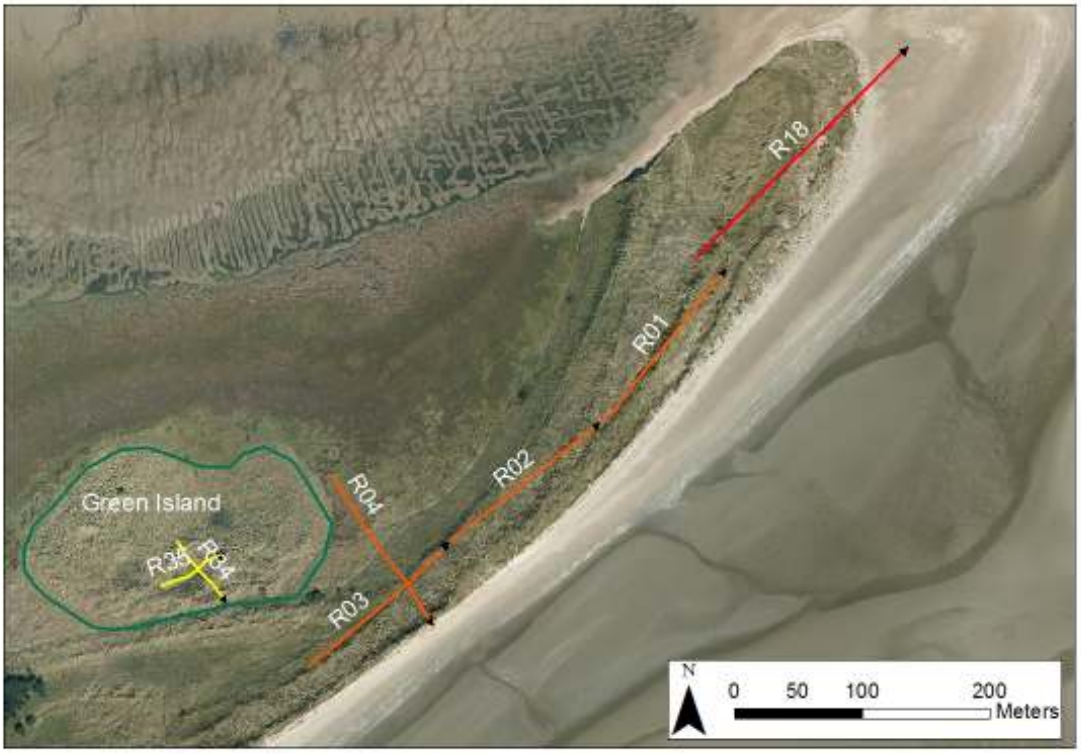

Figure 3.3 – Location of Resistivity lines with 10 m (red), 5 m (orange) and 2 m (yellow) spacingrecorded in Bull Island - Site 1.

Profiles Bull-01-5m, Bull-02-5m and Bull-03-5m run sub-parallel to the younger sand dunes recorded along the north tip of the island, whereas Bull-04-5m, cuts across them. A fence diagram illustrating the resistivity spatial distribution is presented in Figure 3.4. Non-saturated sand dunes are represented by resistivity values over 600Ωm recorded along the surface in profiles Bull-01/02/03-5m and from x-position 70 m onwards in Bull-04-5m. Medium resistivities dominating the region between 2m and 3 m below

OD, depicted along profiles 1, 2 and 3 and at x-position 90 – 130 m are interpreted as a fresh water saturated region. The presence of relatively large sand dunes in this area, reaching altitudes of over 6 m OD permits the development of a shallow freshwater aquifer (at the surface in the Alder Marsh area) along the sand dunes overlying the saline domain region. Saline domain shows resistivity values below 30Ωm depicted in all the profiles parallel to the dunes at approximately 3 m below OD and reaching the surface in Bull-04-5mat x-positions 0 – 70 m, illustrating the salt marsh setting located north-westwards from the sand dunes.

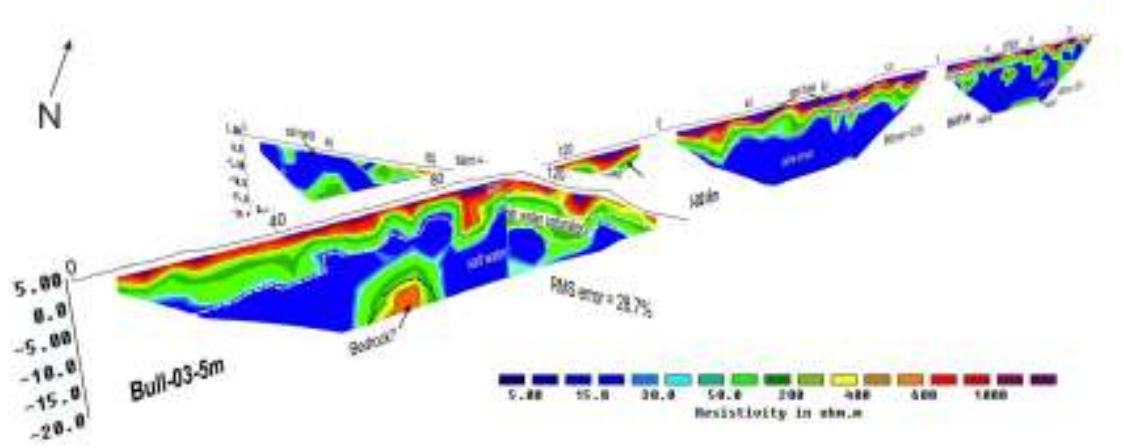

Figure 3.4 – Fence diagram of interpreted resistivity profiles Bull-01-5m, Bull-02-5m, Bull-03-5m and Bull-04-5m with an electrode spacing of 5 m.

Profiles Bull-34-2m and Bull-35-2m (Figure 3.5) are collected in a patch of circular dunes surrounding a depression, named “Green Island” and preceding the development of the longitudinal sand dune cordons dominating the north parts of Bull Island. Its formation has been dated pre-1869 (Harris, 1977). Medium to high resistivity values (500 –1200Ωm) depicted in both profiles in the higher ground areas are associated with sand dunes reaching maximum heights of 3 m above the surrounding landscape. Low to medium resistivity (30 – 200Ωm) is recorded along the surface in the lower ground area and below the sand dune deposits; these are interpreted as fresh water saturated soft sediments, probably composed of aeolian sands overlying marine deposits. These values are underlain by a region dominated by low resistivity values (< 30 Ωm) interpreted as the saline domain.

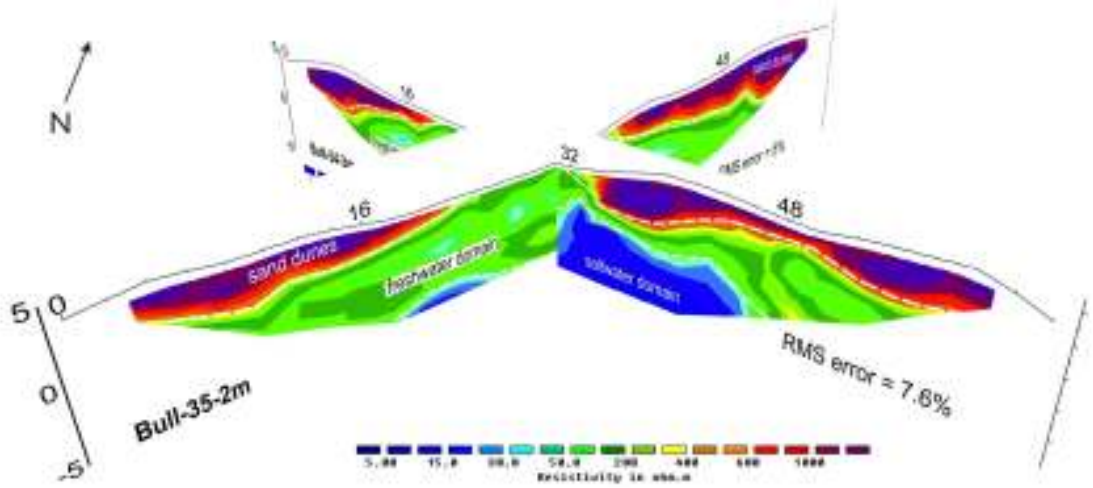

Figure 3.5 – Fence diagram of interpreted resistivity profiles Bull-34-2 m and Bull-35-2m located in Green Island with an electrode spacing of 2 m.

Profile Bull-18-10m (Figure 3.6) is located north of the 5 m spacing profiles (Figure 3.3). Medium to high resistivity values (200 – 1200Ωm) depicted along the surface illustrate the sand dune deposits. Fresh water saturated domain is expressed by medium resistivity values (30 – 200Ωm). A generally low resistivity area showing values below 50Ωm is interpreted as saline domain at depth between 5 and 15 m below OD and coming to the surface from x-position 210 m onwards, where beach sediments take place (Figure 3.3). A medium to high resistivity region (>300Ωm) at x-positions 90 – 155 m and 180 – 200 mis interpreted as bedrock composed of Limestone and Shale (see McConnell et al., 1994). This relatively high resistivity region is flanked by two very low resistivity anomalies, which is possibly caused by the presence of saturated weathered bedrock regions. RMS error was very high on this line.

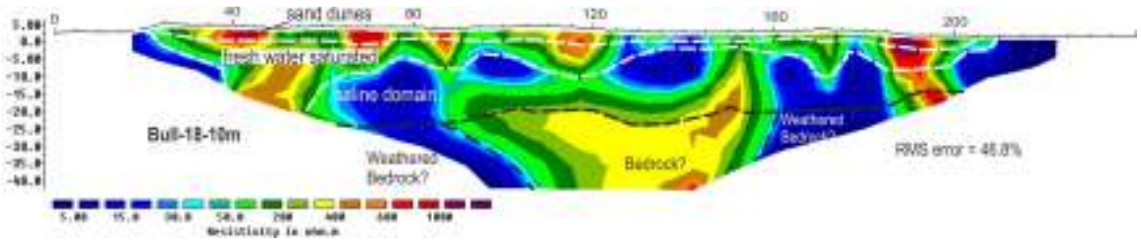

Figure 3.6– Interpreted resistivity profile Bull-18-10m with an electrode spacing of 10 m.

Four main resistivity signatures were differentiated in Site 1 of Bull Island (Figure 3.7). Sand dunes located along the surface are characterised by resistivity values over 400Ωm, these are underlain by medium resistivities at depths in places of 3 m below OD illustrating the presence of a shallow aquifer associated with the sand dune complex. Saline domain, characterized by resistivity values below 30 Ωm, is depicted as a generally continuous zone, recorded at depth in the areas with sand dunes and at the surface in the regions dominated by salt marsh and beach deposits. Bedrock is not proved in this area, however, it is estimated from medium to high resistivities clearly depicted in Bull-18-10m and inferred in Bull-01/03-5m at depths ranging between 15 and 25 m below OD.

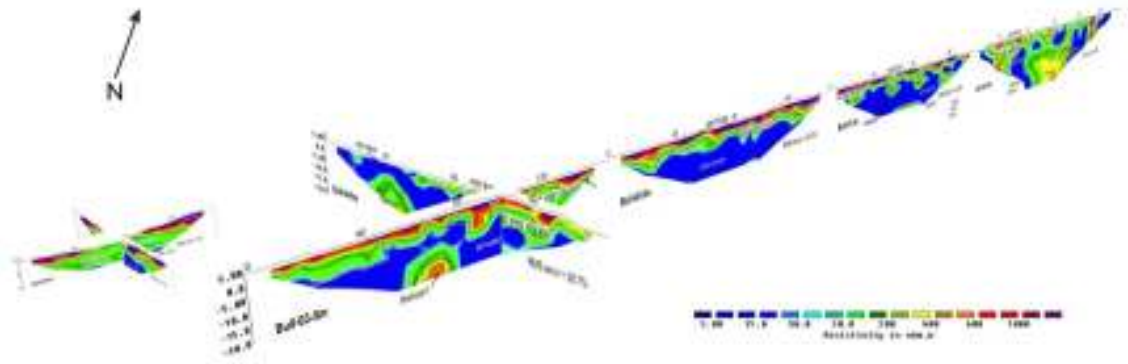

Figure 3.7 – Fence diagram illustrating the 3D spatial distribution of all the resistivity profiles recorded in Bull Island - Site 1.

Bull Island - Site 2

The eight profiles with 5 m spacing and two with 10 and 2 m spacing recorded in Bull Island - Site 2 are presented and described below (Figure 3.8). These data allow a broad characterization of the existing lithological and aquifer types in the central area of Bull Island.

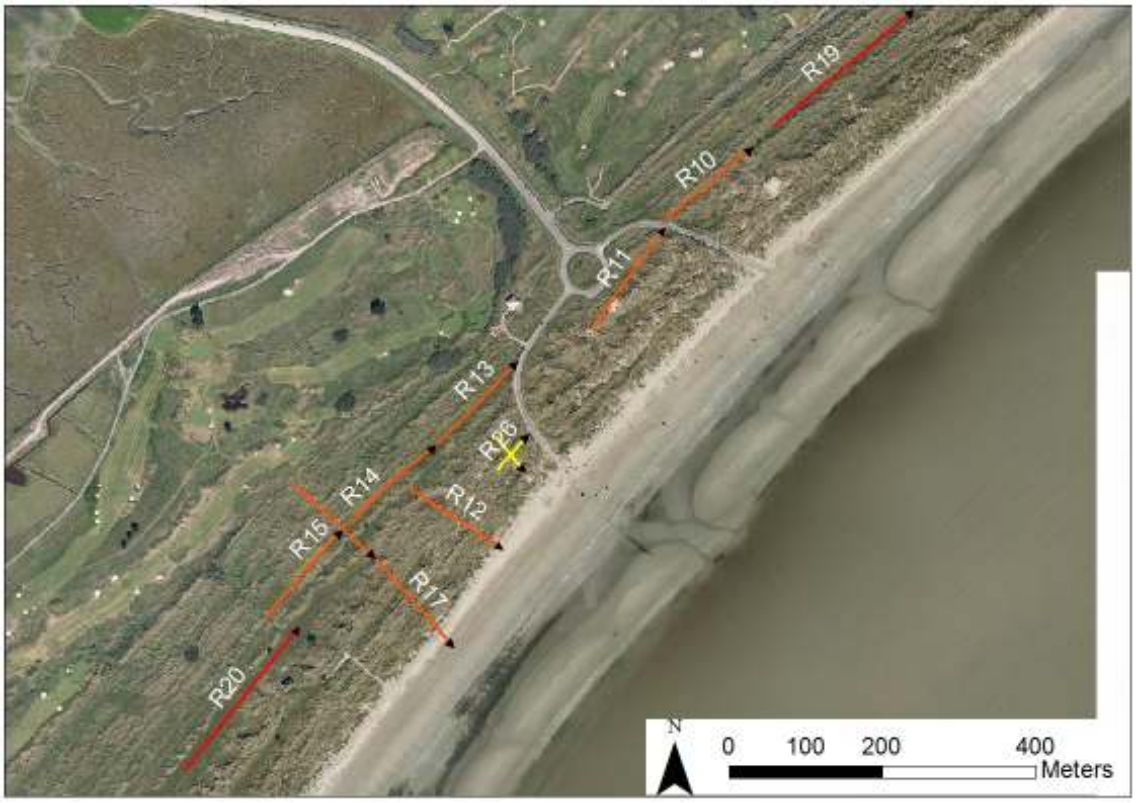

Figure 3.8 - Location of Resistivity lines with 10 m (red), 5 m (orange) and 2 m (yellow) spacing recorded in Bull Island - Site 2.

Profiles Bull-10-5m and Bull-19-10m run along the dune slacks, Bull-11-5m cuts across a series of chaotic sand dune ridges with a blowout like morphology. This profile shows resistivity values over 600Ωm illustrating the sand dune ridges, whereas the profiles recorded in the dune slacks show lower resistivity values along the surface (50 - 300Ωm). A generally homogeneous resistivity layer reaching depths of up to 8 m and presenting resistivities between 30 and 200Ωm below OD is interpreted as fresh water saturated sediments. This is underlain with and undulating contact by a low resistivity area (<30Ωm) disturbed in places by medium resistivities interpreted as artefacts. Finally, medium resistivities with values over 100Ωm underlying the saline domain layer at depths over 20 m below OD are tentatively interpreted as bedrock (Figure 3.9).

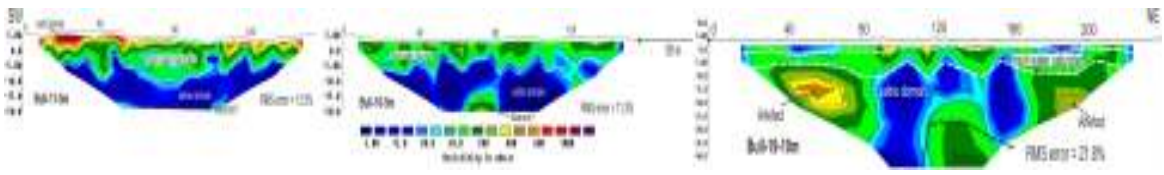

Figure 3.9 –Interpreted resistivity profiles Bull-10-5m, Bull-11-5m, Bull-19-10m with an electrode spacing of 5 m and 10 m.

Profiles Bull-13-5m, Bull-14-5m and Bull-15-5mrun along the dune slacks, whereas Bull-12-5m, Bull-16-5m and Bull-17-5m cut across the sand dune ridges. The former present a low-medium resistivity layer along the surface (50 - 200Ωm) indicative of fresh water saturated soft sediments, the latter show some areas with medium high resistivities (30 and 800Ωm) corresponding with unsaturated sand dunes underlain by low-medium resistivity values corresponding with the fresh water saturated domain. A low resistivity region (<30Ωm) underlying these depicted in all the profiles is interpreted as soft sediments saturated with saline water. The contact between the fresh water and the saline water domains is particularly irregular; this could either be caused by sudden changes on the soft sediment texture controlling the distribution of salty and fresh waters or by the presence of anthropogenic artefacts. Medium resistivities with values over 100Ωm underlying the saline domain layer at depths over 18 m below OD are tentatively interpreted as bedrock (Figure 3.10).

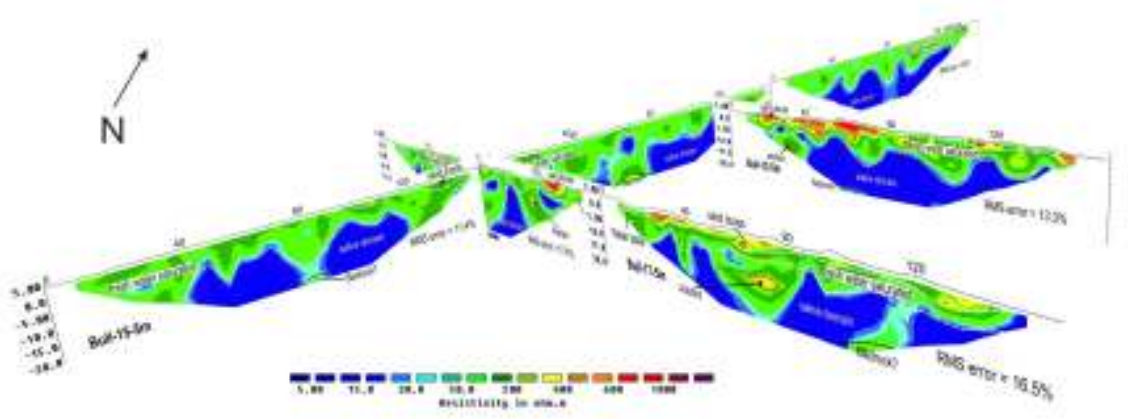

Figure 3.10 –Fence diagram of interpreted resistivity profiles Bull-12-5m, Bull-13-5m, Bull-14-5m, Bull-15-5m, Bull-16-5m and Bull-17-5m with an electrode spacing of 5 m.

Two 2m spacing profiles were collected along (Bull-26-2m) and across (Bull-27-2m) the crest of asand dune (Figure 3.11). Medium to high resistivity values (500 – 1200Ωm) depicted along the top 2 – 5 m correspond to unsaturated sand dunes. A continuous 5 m thick layer underlying the sand dunes showing low to medium resistivity (30 – 200Ωm) is recorded in both profiles at depths over 3 m and at the

surface in profile Bull-27-2m at x-position 44 – 50 m (dune slack), this is interpreted as fresh water saturated soft sediments, probably composed of aeolian sands overlying marine deposits. This region is underlain by a continuous layer dominated by low resistivity values (< 30 Ωm) and interpreted as the saline domain. The contact between the freshwater and the saline aquifers is clearly depicted as a sharp contact at an elevation of 3 m below OD.

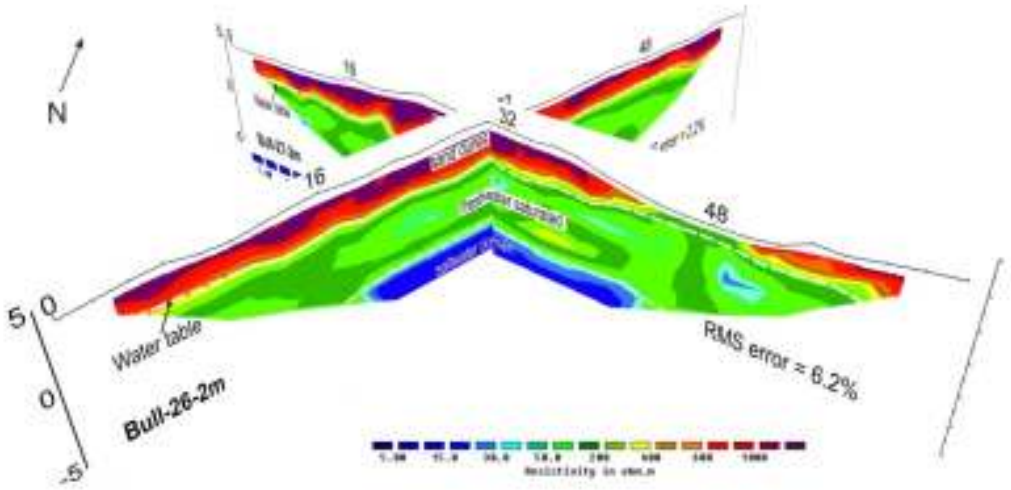

Figure 3.11–Fence diagram showing resistivity profiles Bull-26-2m and Bull-27-2m.

Profile Bull-20-10m (Figure 3.12) runs along a dune slack partially coveredby fresh water marsh deposits. A continuous layer along the surface 4 – 8 m in thickness showing low-medium resistivity values (30 – 200Ωm) corresponds with the fresh water saturated domain expressed on the surface as occasional stretched fresh water pools confined within the dune slack area (Figure 3.1). This is underlain by a continuous layer encompassing resistivity values below 30Ωm corresponding with the saline domain regionencompassing a thickness of over 20 m. Underlying these, alow to medium resistivity layer at depths 30 m below OD (50 - 300Ωm) is interpreted as the bedrock, composed of limestone and shale in this area (McConnell et al., 1994).

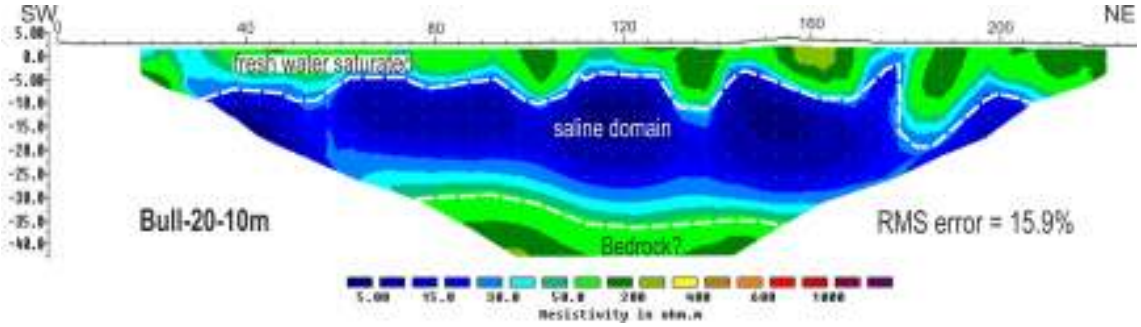

Figure 3.12 – Interpreted resistivity profile Bull-20-10m with an electrode spacing of 10 m.

Four main resistivity signatures were defined in Site 2 of Bull Island (Figures 3.9 and 3.13). Sand dunes dominating the higher ground areas are characterised by resistivity values over 400Ωm. Low to medium resistivities at the surface on the dune slack region and generallyreaching depths of 4 m below OD illustrate the presence of a fresh water shallow aquifer associated to the sand dune complex. Saline domain, showing resistivity values below 30 Ωm is depicted as a generally continuous domain, recorded at depths of 4 m below OD in the sand dunes and at the surface in the area dominated by beach sediments (Bull-17-5m – x-position 145 m). Bedrock is not proved in this area, however, the 10 m spacing profiles (Bull-19/20-10m) show generally continuous medium resistivity layers underlying the saline domains, which are interpreted as bedrock elevation at 28-35 m below OD.

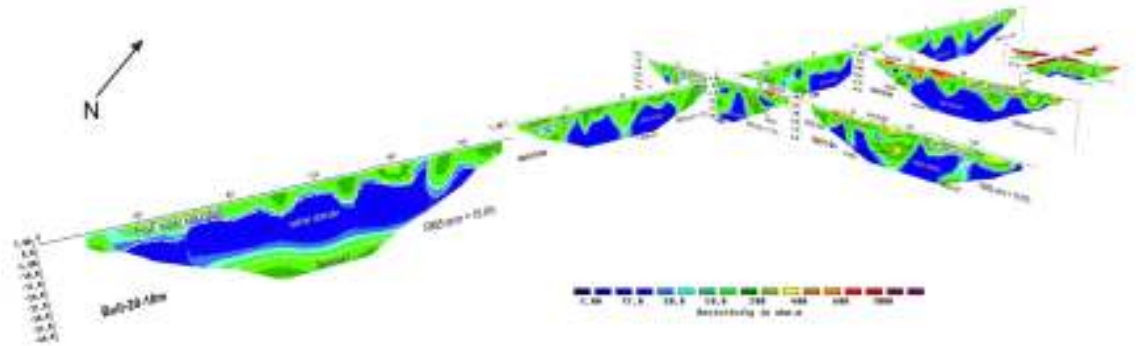

Figure 3.13 – Fence diagram illustrating the 3D spatial distribution of the resistivity profiles south of the road recorded in Bull Island - Site 2.

Bull Island - Site 3

Eight resistivity profiles recorded in Bull Island - Site 3 are presented and described below (Figure 3.14). These datasets allowed for a broad characterization of the existing lithological and aquifer types of the Bull Island southernmost region.

Figure 3.14 – Location of Resistivity lines with 10 m (red), 5 m (orange) and 2 m (yellow) electrode spacing recorded in Bull Island - Site 3.

Bull-06-5m and Bull-05-5m run parallel and across the sand dunes in south Bull Island. A fence diagram illustrating the resistivity spatial distribution is presented in Figure 3.15. Non saturated sand dune deposits illustrated by resistivity values over 400Ωm are recorded in some areas along the surface of both profiles. These high values are intercalated with areas showing low-medium resistivities extending to depths over 5 m below OD. The saline domain is illustrated by a generally continuous level 12 – 15 m in thickness with resistivity values below 30Ωm. Depth to bedrock is estimated at 17 m below OD from a low-medium resistivity layers (50 - 200Ωm) recorded at the lower regions of both profiles.

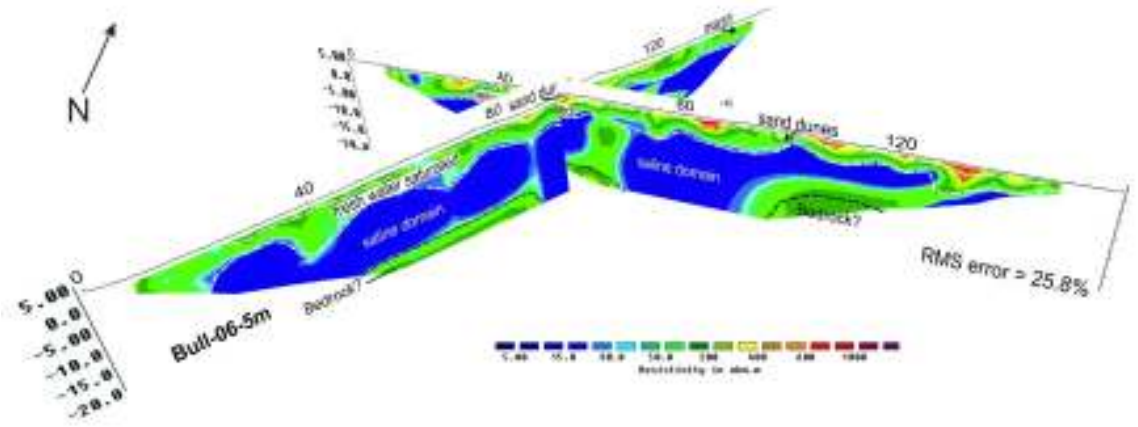

Figure 3.15–Fence diagram showing resistivity profilesBull-05-5m and Bull-06-5m.

Profiles Bull-07-5m, Bull-08-5m and Bull-21-10m run along a large fresh water marsh area situated landward from the most prominent sand dune system; Bull-09-5m cuts across this sand dune system running seaward from the freshwater marsh. Medium to high resistivities values (300-800Ωm) corresponding with non-saturated sand dunes are recorded along the surface in Bull-09-5m from x-position 65 m onwards. Profiles running along freshwater marsh deposits show a low-medium resistivity layer along the surface (50 - 200Ωm) which extends at depths over 3 m below OD. A generally continuous low resistivity region(< 30Ωm) in Bull-07/09-5m and discontinuous in Bull-08-5m and Bull-21-10m underlying the shallow freshwater aquifer is interpreted as soft sediments saturated with saline waters. The contact between the fresh water and the saline domain is particularly irregular in the northern profiles; this could relate either to sudden changes on the soft sediment texture controlling the distribution of salty and fresh waters or tothe presence of anthropicartefacts. Medium resistivities with values over 100Ωm underlying the saline domain layer at approximately 20 m depth below OD may be bedrock (Figure 3.16).

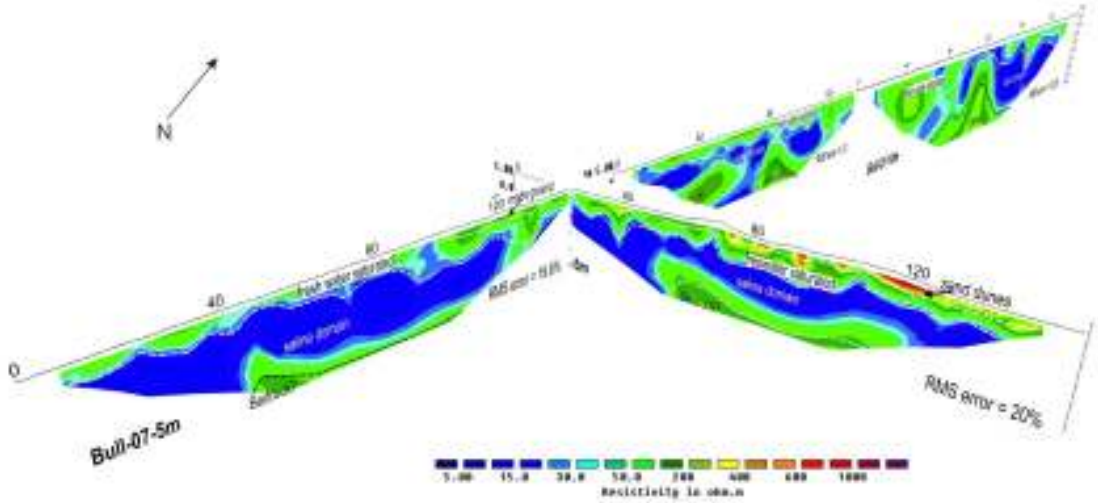

Figure 3.16–Fence diagram showing resistivity profiles Bull-07-5m, Bull-08-5m, Bull-09-5m and Bull-21-10m.

Two 2m spacing profiles were collected along (Bull-36-2m) and across (Bull-37-2m) embryonic sand dunes (Figure 3.17). Profile Bull-36-2m shows high resistivity values (>400Ωm) associated with the foredune system and low resistivities (15 – 40Ωm) corresponding with embryonic sand dunes. Long section of embryonic sand dunes are characterized by low-medium resistivities (15 – 200 Ωm), medium resistivities recorded in Bull-37-2m at x-positions 32 – 56 m are underlain by a 2.5 m thick continuous layer with low resistivity which has continuity at the surface at x-positions 0 – 32 m. These low resistivity layer is underlain by a continuous 5 m thick higher resistivity layer (50 – 200 Ωm), this is expressed in Bull-36-2m as a relatively high resistivity wedge connected to the sand dune system behind the embryonic sand dunes and probably corresponding with a freshwater shallow aquifer associated with the sand dune system. Finally, a low resistivity layer (10 – 30Ωm) at depths of 5 m below OD in Bull-37-5m is likely associated with the saline domain.

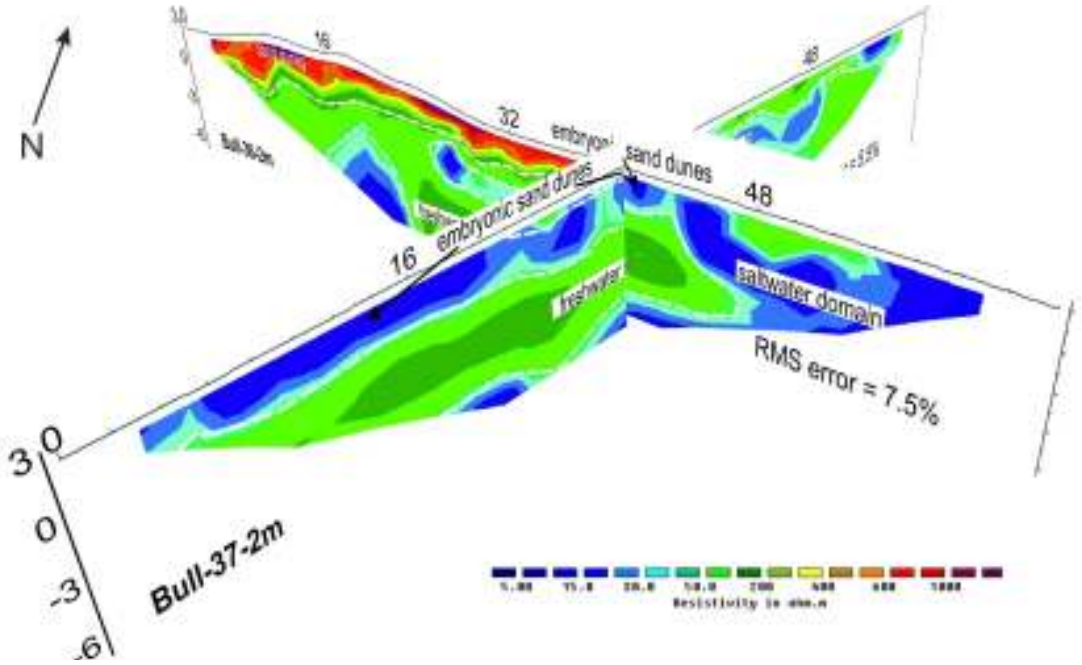

Figure 3.17–Fence diagram showing resistivity profilesBull-36-2m and Bull-37-2m.

Four main resistivity signatures are depicted in Bull Island – Site 3 (Figures 3.18). Sand dunes dominating the higher ground areas are characterised by resistivity values over 400Ωm. Low to medium resistivities recorded at the surface on fresh water marsh deposits and reaching depths of more than 4 m below OD correspond to fresh water shallow aquifer associated with the sand dune complex. Saline domain is depicted as a generally continuous layer with resistivity values below 30 Ωm recorded at depths 4 m below OD in the sand dunes areas and at the surface in the areas dominated by beach deposits and embryonic dunes (Bull-37-2m – x-position 0 - 32 m). Medium resistivity layers recorded on the 5 m and 10 m electrode spacing profiles underlying saline domain areas are interpreted as bedrock at depths 14 - 17 m below OD, somewhat in agreement with borehole records from Dublin Port located 300 and 400 m southwest from the site presenting a presumed rock head elevation of 13 m below OD.

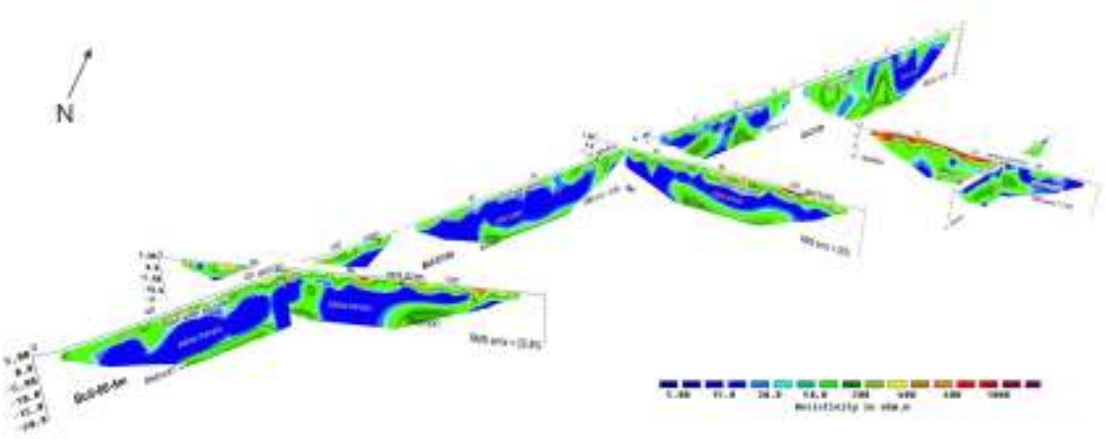

Figure 3.18 – Fence diagram illustrating the 3D spatial distribution of the resistivity profiles in Bull Island - Site 3.

3.2.1.2. Ground Penetrating Radar

The radar facies stratigraphy concept presented by Neal (2004) allows the construction of a relative chronology within GPR radargrams as well as with adjacent ones. The terminology for description of the radar signatures and the description and classification of radar facies presented within this work is based on Neal's (2004) coding scheme (Figure 3.19). The interpretation coding format has been adapted and modified for this project by adding a number of sedimentological and structural codes specific of coastal environments (Bristow et al., 2000; Neal et al., 2002). The coding scheme attempts to represent the potential situations presented by aeolian, marine and estuarine environments existing in the Bull Island area and glacial, glaciofluvial and glaciolacustrine recorded in the Killiney beach section.

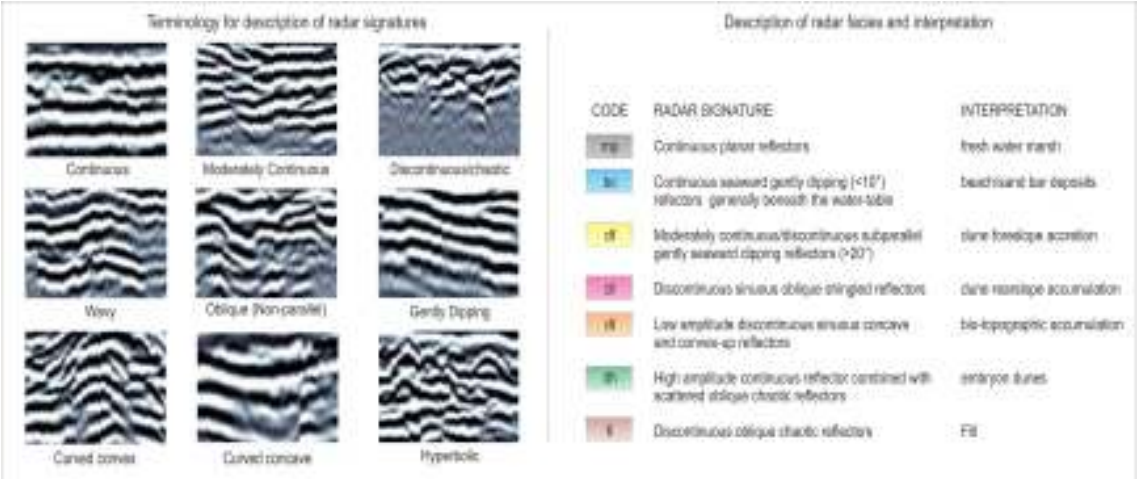

Figure 3.19 – Left – Terminology for description of radar signatures, samples shown are extracted from radargrams collected during this project. Right — colour scheme for radar facies description and interpretation modified from Bristow et al. (2000) and Neal (2004),

Bull Island - Site 1

Site 1 comprises two remarkable geomorphological features: (i) a complex composed of subparallel dune ridges evolving northeastwards into a recurve fan shaped ridge system and; (ii) Green Island, an area constituted bycircular shaped sand dunes illustrating the palaeo-coastline previous to 1869, as recorded in the the O.S. maps (Harris, 1977). The two most landward sand dune ridges diverge south of the site and converge again east from Green Island, where the youngest ridge truncates the older. A closed depression located between those ridges allowed for the development of a fresh water marsh (Alder Marsh) of significant ecological value. North of Green Island the foredune ridge diverges out into several ridges forming the recurve at the northeast end of Bull Island. Fourteen GPR profiles were recorded in the site in order to investigate the internal architecture of these features (Figure 3.20).

Figure 3.20 – Location of GPR profiles collected in Bull Island – Site 1.

Five radar facies are recognized on the basis of reflection character and geometry, the interpretation is based on the recorded signatures and the geomorphology of the area (Figure 3.1 and Figures 3.21 and 3.22). Sand dunes in Green Island region show circular foredune development (Figure 3.21), confirming this island was formed independently at an earlier stage than the parallel dune ridges to the east, the oldest of those truncates the Green Island south palaeo-coastline, the truncation is expressed as a continuous reflector dipping southeast depicted at x-position 155 – 175 m in Bull 19 and interpreted as an erosional contact illustrating the palaeo-coastline at the time this dune ridge was acting as a foredune (Figure 3.23). Dunes to the southeast of it formed at a later stage and merge to the east of Green Island as a single ridge, which diverge again to the northeast from this point giving way to four ridges at the recurve area. These parallel converging/diverging ridges accommodate to the tidal wave regime. The single foredune where the dunes converge in and diverge from is currently dominated by erosional processes compensating for sand deposition, which do not allow coastal accretion in this area. North-eastwards, the sand dunes diverge out forming the recurve in a series of sand dunes dominated by reflectors dipping towards the southeast at up to 20° and interpreted as foreslope accretion sediments (Figure 3.24). Some reflectors

dipping towards the backslope of the dune are interpreted as rearslope deposits. Bio-topographic accumulation facies are quite common in the slack dune areas and/or in regions where sand accumulation shows very poor topographic expression. Continuous horizontal reflectors along areas with poor topographic expression depicted on GPR lines Bull-18,19,20,22 are interpreted as fresh/salt water marsh deposits. Finally, reflectors dipping gently southeastwards generally developing below the water table are interpreted as marine beach/sand bar deposits.

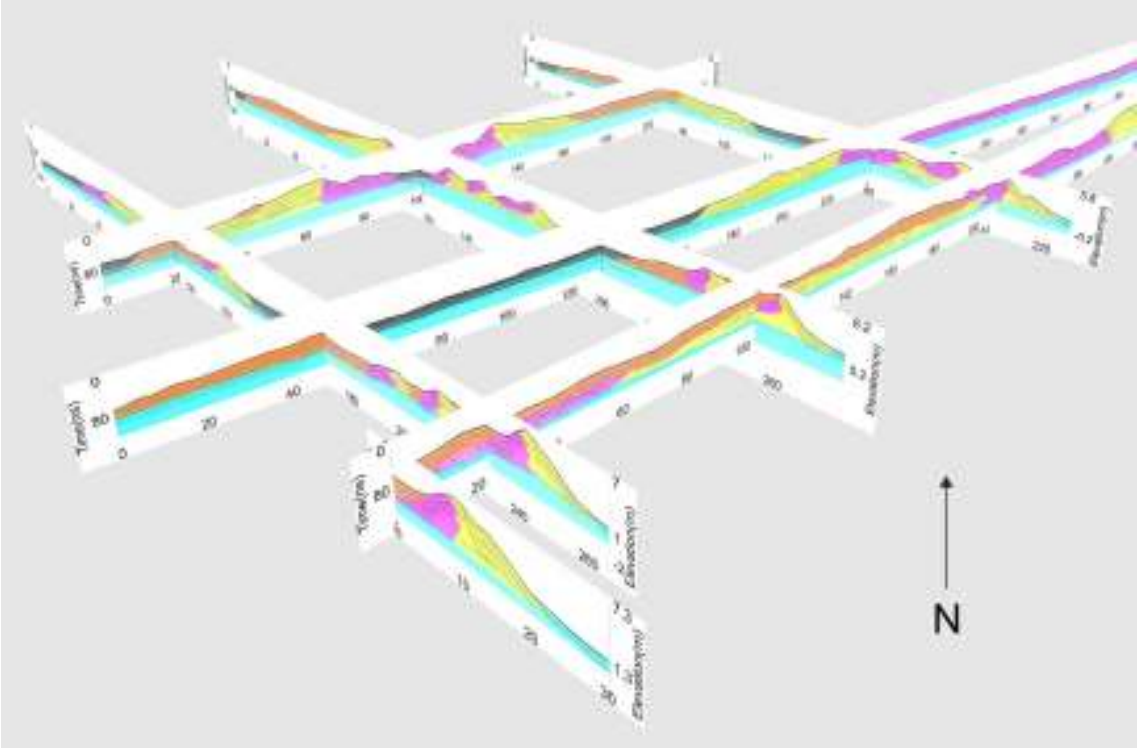

Figure 3.21 – Fence diagram illustrating interpreted GPR profiles collected in Bull Island – Site 1, Green Island.

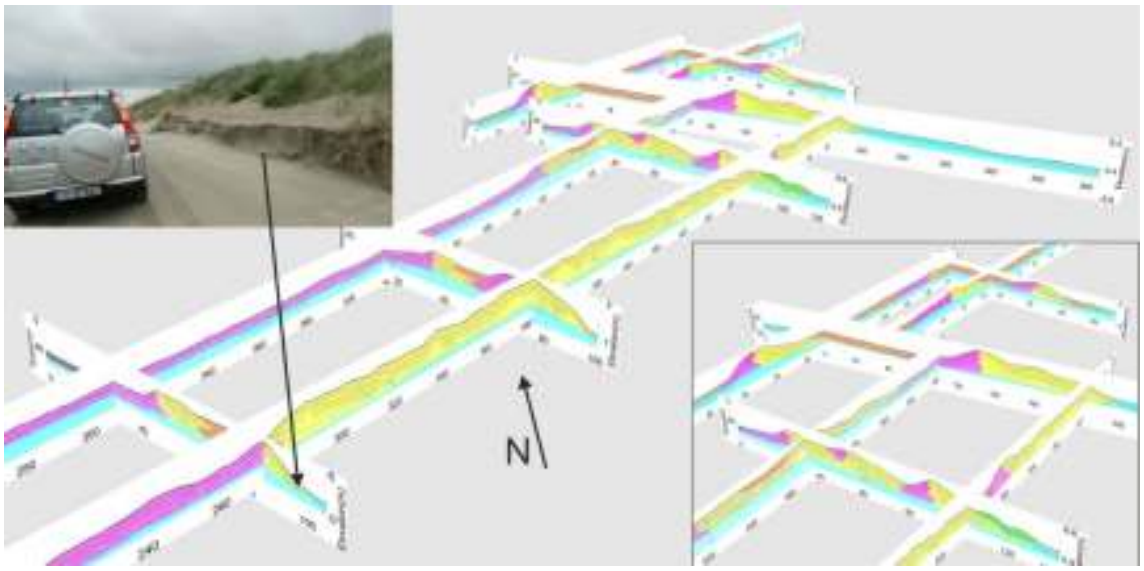

Figure 3.22 – Fence diagram illustrating interpreted GPR profiles collected in Bull Island – Site 1, in the recurve area with a zoom of the northeast part. Photograph illustrates intensive erosional processes along profile 24 associated with high tide two days after the survey.

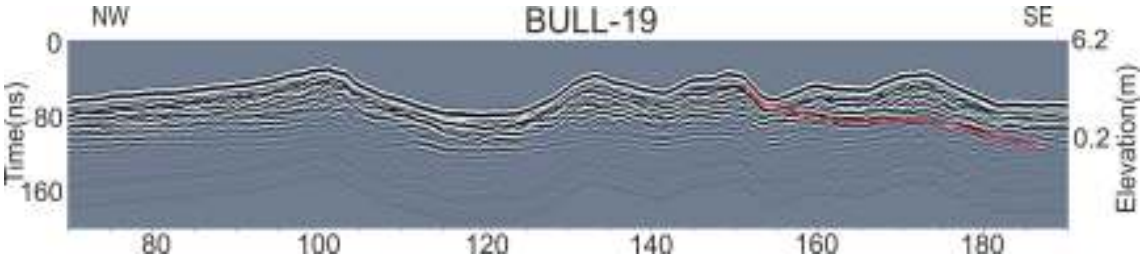

Figure 3.23 – Radargram illustrating sand dunes radar facies in Green Island area. Red line indicates position of the coast before growth of the sand dune truncating Green Island.

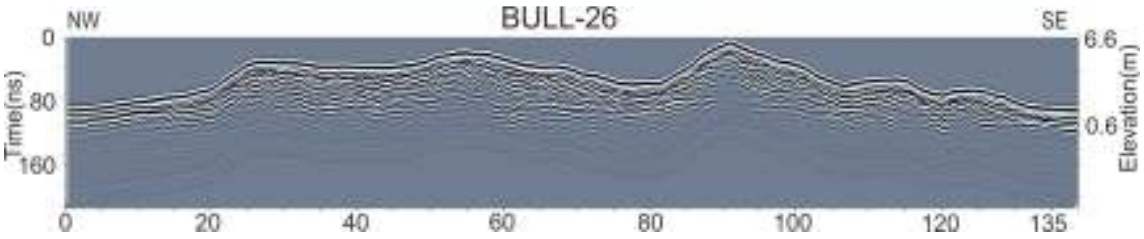

Figure 3.24 – Profile 26 illustrates cross section of three sand dunes constituting the recurve.

Bull Island – Site 2

Eight radargrams cutting across each other were recorded in the site forming a grid (Figure 3.25). Four profiles run parallel to the dune ridges direction from southwest to the northeast and four cut the dune ridges orthogonally from northwest to southeast.

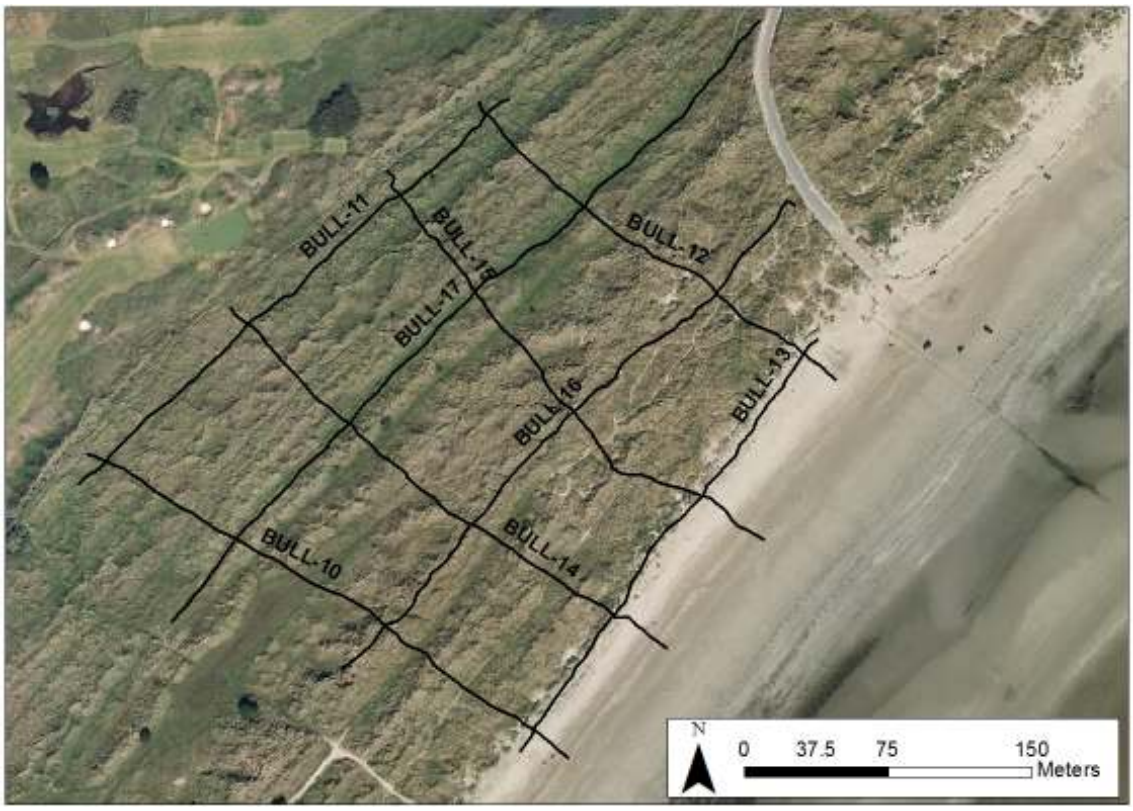

Figure 3.25– Location of GPR profiles collected in Bull Island – Site 2.

Six radar facies are recognized on the basis of reflection character and geometry, the interpretation is based on the recorded signatures and the geomorphology (Figure 3.26). Sand dunes in this area consist of well-developed sub parallel ridges with an average height of 2 – 3 m above the slack areas. Profiles orthogonal to the dunes cut across approximately ten individual dune ridges separated by slack areas covered in places by narrow minor fresh water marsh sediments. Embryonic dunes are recorded all along the seaward side of the foredunes system as chaotic discontinuous reflectors (Figure 3.27). The dunes are generally composed of foreslope and rearslope accretion deposits, the slacks between slopes are either composed of interstratified foreslope and rearslope deposits and/or bio-topographic accumulation deposits. However, reflectors dipping up to 18° towards the southeast, interpreted as foreslope accretion units, are dominant (Figure 3.28). A narrow freshwater marsh running along the dunes slack area is depicted at x-position 125 – 135 m in Bull-10. Fresh water marshes are common at the southern

portion of the island becoming more unusual towards this area. Marine sediments expressed as continuous seaward gently dipping moderately continuous reflectors mostly developing beneath the water-table and underlying all the sediments are composed of sand and silty sand (Figure 1.4 – BH-B5) located 1 Km north from the site (Figure1.2).

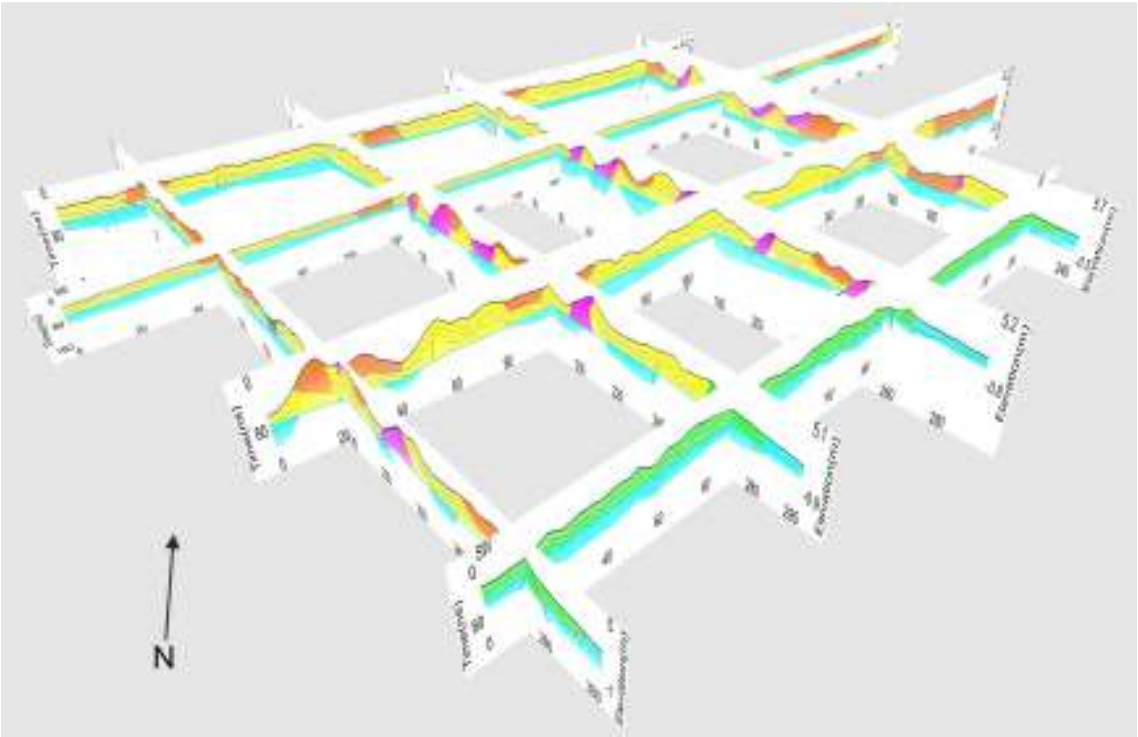

Figure 3.26 – Fence diagram illustrating interpreted GPR profiles collected in Bull Island – Site 2.

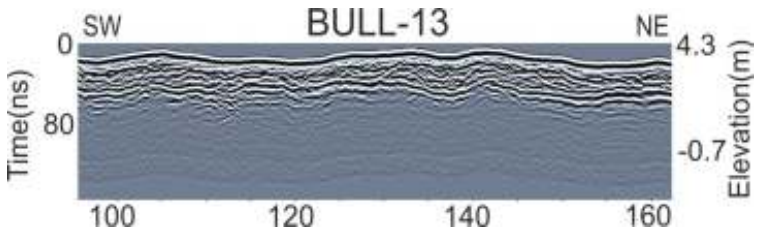

Figure 3.27 – Profile 13 illustrates long section of embryonic sand dunes, poor penetration below water table expressed as a continuous reflector at approx. 2 m OD.

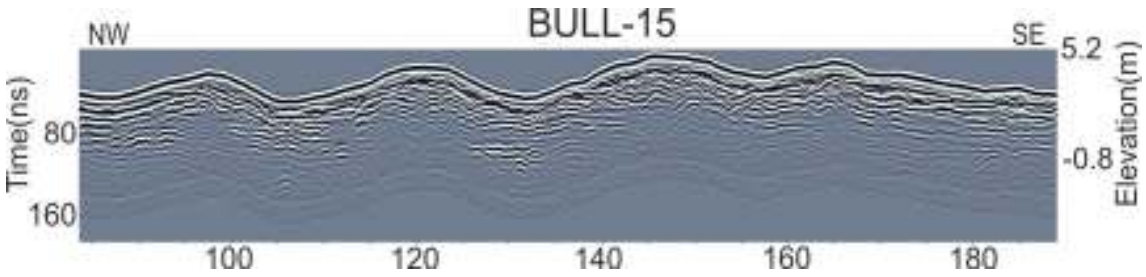

Figure 3.28 – Profile 15 illustrates cross section of four sand dunes developing from NW to SE in Site 2.

Bull Island - Site 3

Eight radargrams cutting across each other were recorded in the site forming a grid (Figure 3.29). Four profiles run parallel to the dune ridges direction from southwest to the northeast and four cut the dune ridges orthogonally from northwest to southeast.

Figure 3.29 – Location of GPR profiles collected in Bull Island – Site 3.

Seven different radar facies are recognized on the basis of reflection character and geometry. Interpretation is based on their signature and the geomorphology (Figure 3.30). Sand dunes in this area show fairly smooth topographic expression and are 2 – 3 m high. Profiles orthogonal to the dunes cut across seven dune ridges in the northeast

region and across four in the southwest area separated by large areas covered by fresh water marsh. Embryonic dunes are recorded all along the seaward side of the foredunes system. Most of the dunes are composed of foreslope and rearslope accretion deposits, the slacks between slopes are either composed of interstratified foreslope and rear-slope deposits and/or bio-topographic accumulation deposits. Large freshwater marshes dominate the southern interdune region thinning towards the northeast (Figure 3.31; x-positions 260 – 290 m). These marshes were probably dominated by saltwater in the past and were gradually recycled into freshwater as the sand dunes advanced seawards and dams were built to prevent sea water flooding during surge tides. Some of the sand dunes present a continuous reflector dipping southeast showing continuity under the water table interpreted as an erosional contact illustrating the former coastline, e.g. Bull-06 at x-positions 10 – 50 m (Figure 3.32). Marine sediments consisting of continuous seaward gently dipping moderately continuous reflectors mostly developing beneath the water-table underlain all the deposits described. These sediments are composed of sand and silty sand and have been recorded in boreholes BH-B1/B2 located southwest from the site (Figure 1.4). Finally, man-made ground consisting of dams built to protect the fresh water marshes from seawater flooding depicted at x-positions 90 – 120 m along profile Bull-07 are characterized by chaotic reflectors.

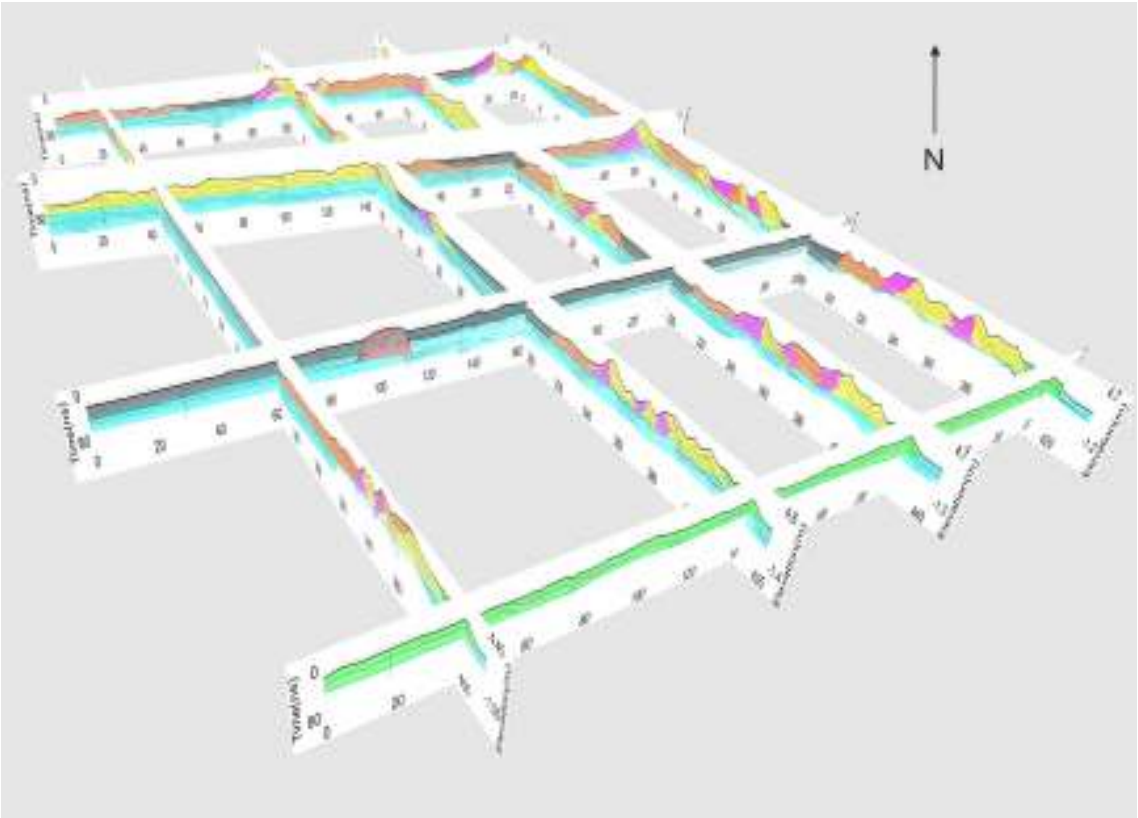

Figure 3.30 – Fence diagram illustrating interpreted GPR profiles collected in Bull Island – Site 3, vertical exaggeration x 2.

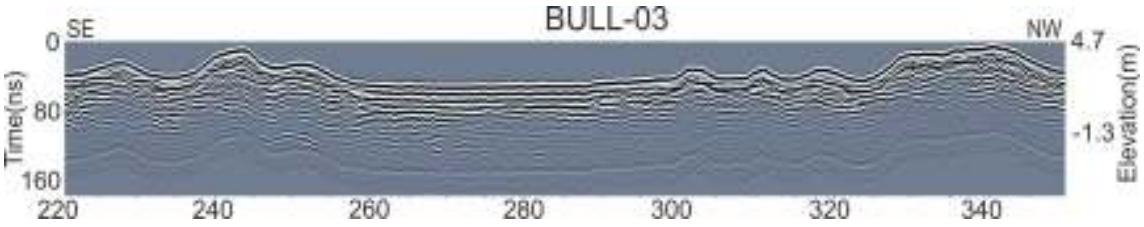

Figure 3.31 – Profile 3 illustrates cross section of sand dunes with an area at x-positions 260 – 290 m dominated by fresh water marsh.

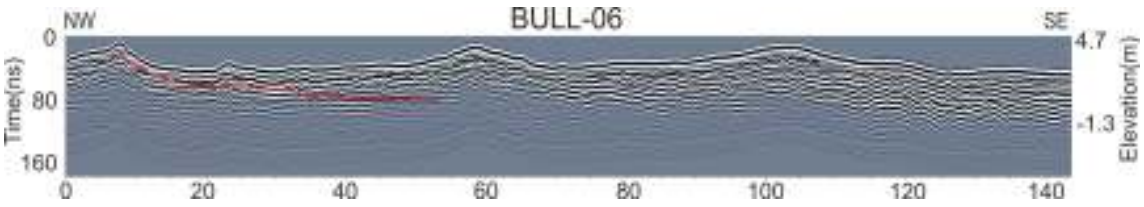

Figure 3.32 – Profile 6 illustrates cross section of sand dunes with erosional contact depicted in red indicating position of the coastline at the time the dune was at the shore.

3.2.2. Killiney Beach

3.2.2.1. Resistivity

Killiney - Site 1

Four resistivity profiles with 10 m electrode spacing recorded in Killiney - Site 1 are presented and described below (Figure 3.33). These datasets allowed for a broad characterization of the existing lithological types in the Killiney area.

Figure 3.33 - Location of Resistivity profiles and BH-1 recorded in Killiney - Site 1.

Two profiles and three borehole records recorded and compiled, respectively by the Shanganagh River are presented in Figure 3.34. Borehole records, located along the south margin of the river bed, show the top 10 m dominated by sand and gravel with lenses of fine sediments corresponding with medium to high resistivities (100 - 800Ωm) recorded along the surface in Kil-23-10m at x-positions 100 – 240 m and in portions of Kil-28-10m. Sand and gravel and clay cobbles and boulders dominate the region between 10 and 30 m depth in BH-K1 (2 – 22 m below OD). This region shows a wide resistivity range in the profiles Kil-23/28-10m: areas with medium to high resistivity (100 - 800Ωm) and large lenses with very low resistivity (< 30Ωm). This probably could be related either to sharp variations in the subsurface sediment distribution propitiating areas of focused saline intrusion or water treatment plant leakage. Bedrock recorded in BH-K1 at 22 m below OD is illustrated in both resistivity profiles by medium to high resistivity (200 - 1000Ωm) dominating the region 20 m below OD.

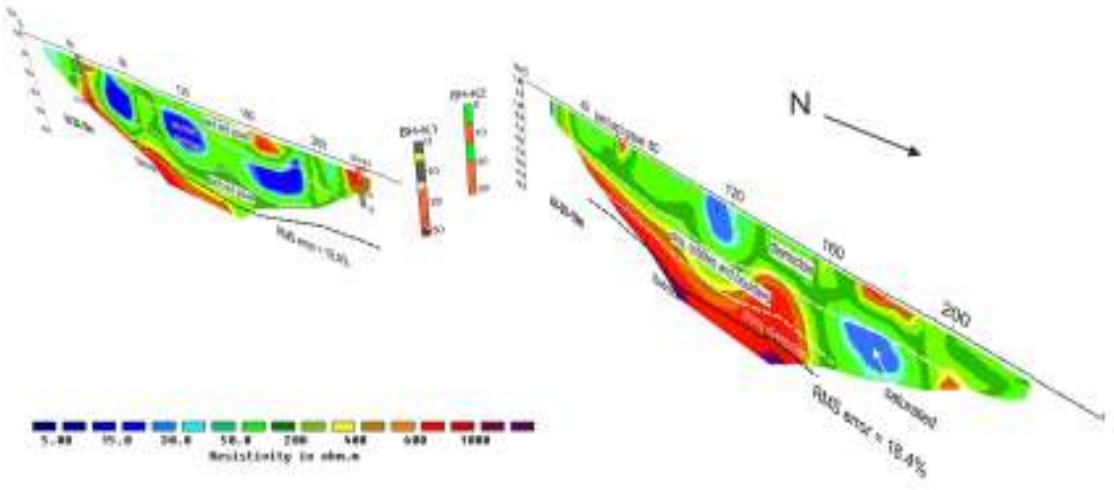

Figure 3.34 –Fence diagram showing resistivity profilesBull-22-10m andBull-28-10m.

Two profiles collected on the higher ground area south of the Shanganagh River valley are presented in Figure 3.35. Profile Kil-23-10m is dominated by low- medium resistivities (50 - 200Ωm) with some large lenses dominated by low resistivity (< 40Ωm) distributed intermittently along the surface and at x-positions 100 – 150 m and 180 – 210 m in the deeper regions. No evidence of bedrock is recorded in this profile. Kil-29-10m encompasses three main continuous horizontal resistivity layers. Medium resistivities (50 - 200Ωm) dominate the top 10 m, these are underlain by a low-medium resistivity layer (30 - 100Ωm) interpreted as saturated diamicton/sand and gravel. Finally, a medium-high resistivity layer (100 - 600Ωm) dominates the area at depths of 20 m below OD, which corresponds with the depth to bedrock recorded in BH-K1 (Figure 1.4).

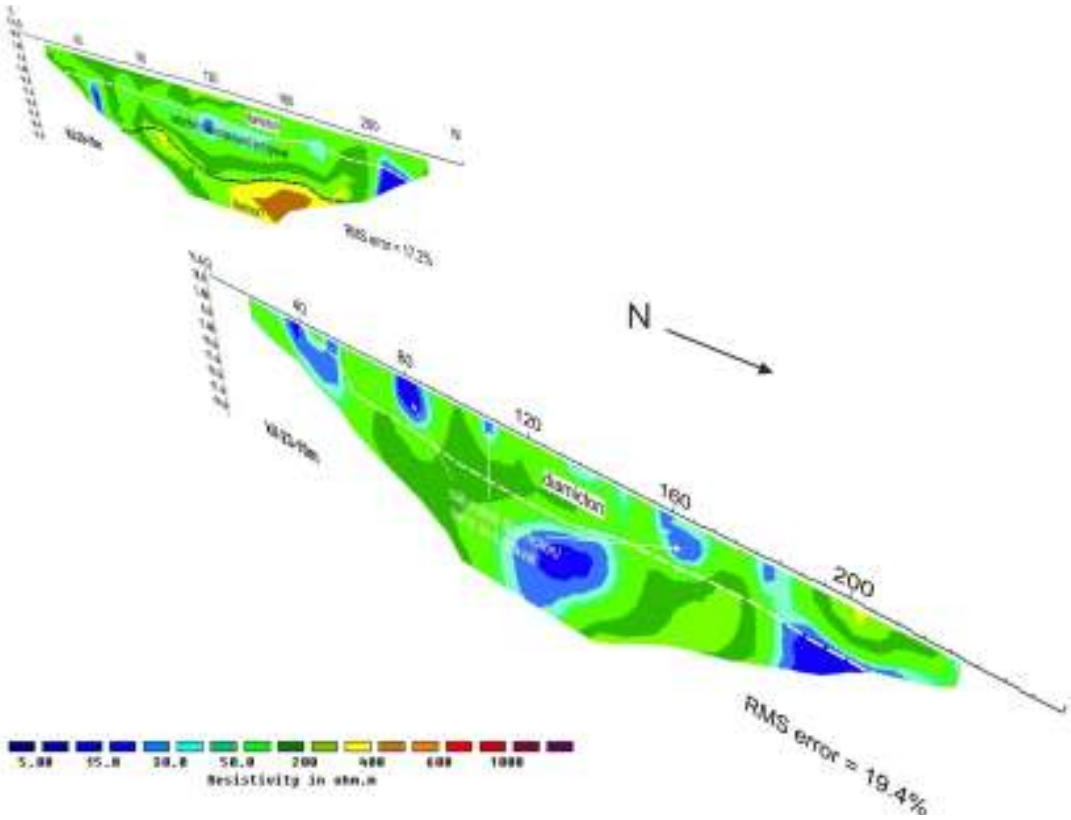

Figure 3.35–Fence diagram showing resistivity profilesBull-23-10m and Bull-29-10m.

Four main resistivity signatures are recorded in Killiney – Site 1: (i) medium to high resistivities (100 - 800Ωm) recorded along the surface and interpreted as sand and gravel deposited along the Shanganagh River Valley; (ii) zones comprising medium to high resistivity (100 - 800Ωm) and large lenses with very low resistivity (< 30Ωm), probably indicating sharp variations in the subsurface sediment distribution; (iii) low-medium resistivities (30 - 100Ωm) interpreted as saturated diamicton/sand and gravel and; (iv) medium-high resistivity (100 - 600Ωm) at depths over 20 m below OD corresponding with bedrock.

Killiney - Site 2

Five resistivity profiles with 10m electrode spacing and a 2.5D model generated from 11 parallel 2D resistivity profiles were recorded in Killiney - Site 2 (Figure 3.36). These datasets allowed for a broad characterization of the existing lithological types in the Quinn's road area.

Figure 3.36 - Location of Resistivity profiles 3D-RES recorded in Killiney - Site 2.

Three resistivity layers are differentiated in Kil-30-10m (Figure 3.37): A 10 m thick layer along the surface at x-positions 60 – 240 m pinching out southwards encompassing resistivities between 50 - 600Ωm and interpreted as sand and gravel/diamicton; a region along the whole profile composed of materials showing low-medium resistivity (50 - 200Ωm) and large lenses dominated by low resistivity values (< 40Ωm) at the surface at x-positions 0 – 60 m and a small medium to high resistivity patch (> 300Ωm) located at 20 m below OD at x-positions 120 – 160 m and inferred as bedrock.

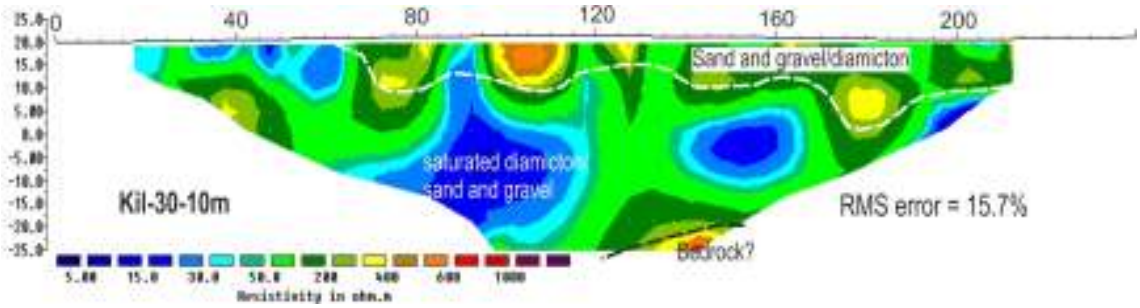

Figure 3.37 – Resistivity profile Kil-30-10m

Two main resistivity regions are depicted along Kil-33-10m (Figure 3.38). The region above 5 m below OD encompasses a series of intercalated lens-like areas with low (<

40Ωm) and high resistivity values (> 400Ωm), these areas are randomly distributed, do not seem to follow apattern of spatial distribution and are probably associated with soft sediments with sharp textural changes influencing the degree of saturation and their resistivity. The area at depths over 10 m below OD at x-positions 70 –110 m encompassing high resistivities (> 600Ωm) is inferred as bedrock.

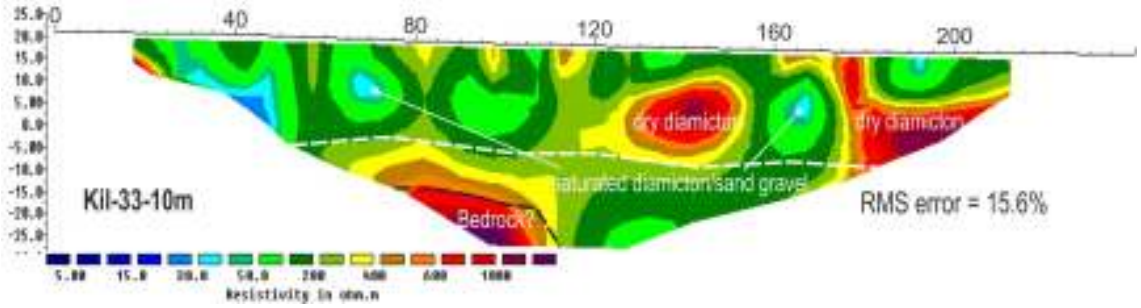

Figure 3.38 – Resistivity profile Kil-33-10m

Three profiles located between the lines described above are presented in Figure 3.39. Medium resistivities (200 - 500Ωm) recorded in 3 – 5 m thick discontinuous layers pinching out towards the margins are interpreted as sand and gravel deposits described along the cliff. These sediments are underlain by generally low-medium resistivity values (100Ωm) with lenses showing low resistivities (<40Ωm), the sediments associated with these resistivities in Kil-24-10m are described along the cliff as clast rich silty diamicton (Rijsdijk et al., 2010) and show seepage in some locations. High resistivity values (>600Ωm) recorded along the lower regions of the three profiles are interpreted as bedrock. These high resistivity areas interpreted as bedrock show sudden lateral changes to low-medium resistivities, which may relate to the nature of metamorphic rocks (gneiss and schist) underlying these area. This pattern is repeated on the profiles orientated south-north (Figures 3.37 and 3.38), whereas in Kil-25-10m, collected west-east, the rock head is recorded as a continuous layer along all the profile gradually dipping eastwards.

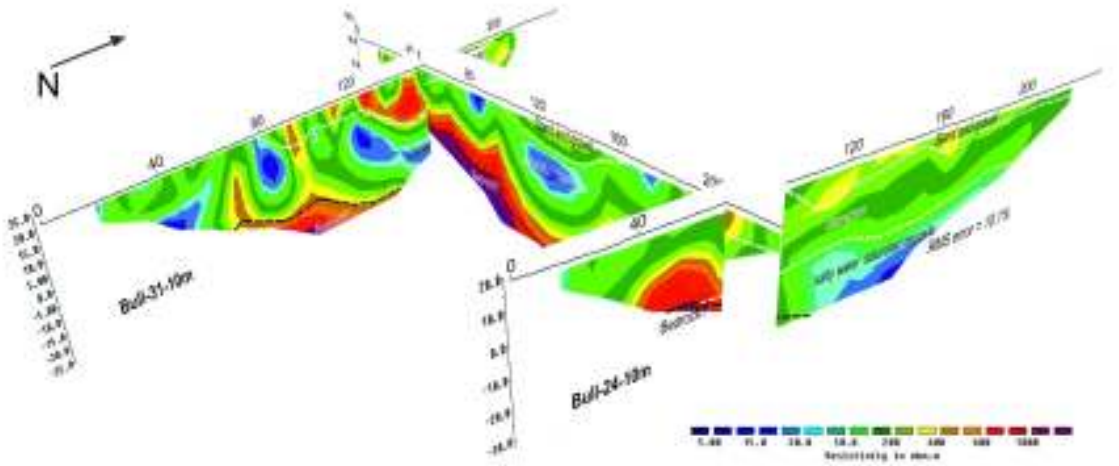

Figure 3.39 – Fence diagram showing profiles Kil-24-10m, Kil-25-10m and Kil-31-10m.

3D – Model

A resistivity 3D model was produced with RES3DINV software using 11 profiles with an electrode spacing of 2 m, orientated south-north, collected parallel to each other with a line-to-line distance of 6 m. The cube dimensions are x-axis = 54 m, y-axis = 60 m and z-axis = 12 m. The relative position of the 3D model versus the 10 m spacing profiles collected in the area is presented in Figure 3.40. High resistivity values along the seaward side of the 3D-RES correspond with resistivity recorded at x-positions 0 – 60 m of Kil-24-10m. 3D-RES depth slices presented in Figure 3.41 shows three main resistivity domains: A thin layer along the surface pinching out north-eastwards and thickening to the southwest encompassing resistivity values over 200Ωm is interpreted as sand and gravel; this is underlain by a low resistivity layer (15 – 70 Ωm) corresponding with sandy silty diamicton recorded along the cliff; The lowest region at depths over 5 m are dominated by medium to high resistivities (>200Ωm), which have been interpreted as sand and gravel as recorded along the cliff (See sedimentary log 23 in Figure 2 in Rijsdijk et al., 2010). The 3D model allows an estimation of the true dip of the layers recorded, apparent dips pointing southwards recorded in the cliff by Rijsdijk et al. (2010) are confirmed as layers with a true dip towards the southwest after visual analysis of the 3D-RES cube (See Figure 3.41).

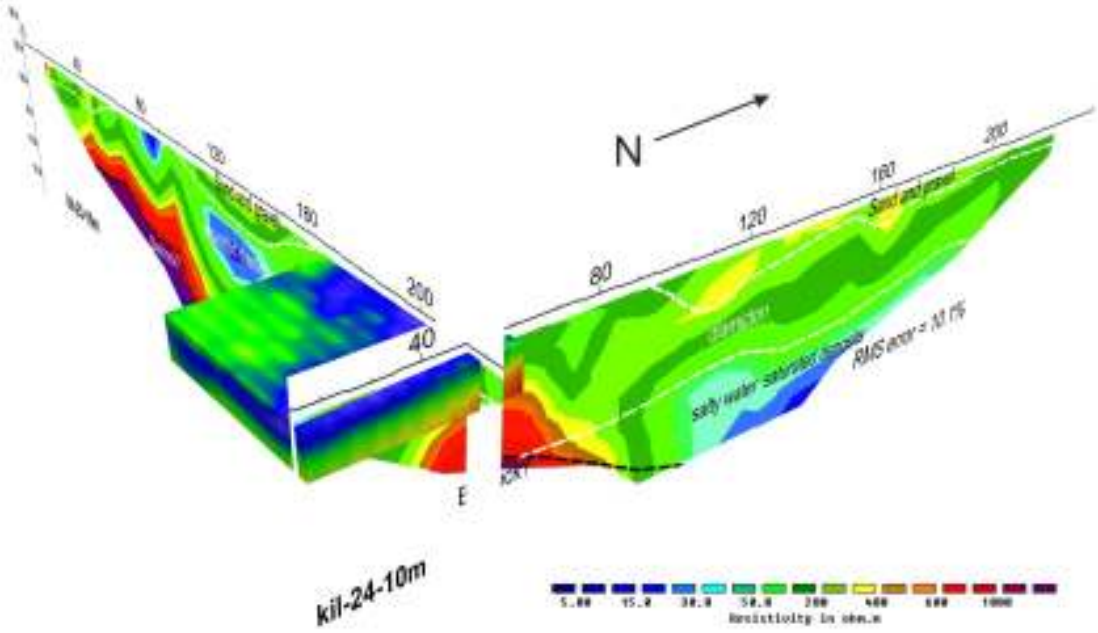

Figure 3.40 – Fence diagram showing profiles Kil-24-10m and Kil-25-10m resistivity 3D Model 3D-RES.

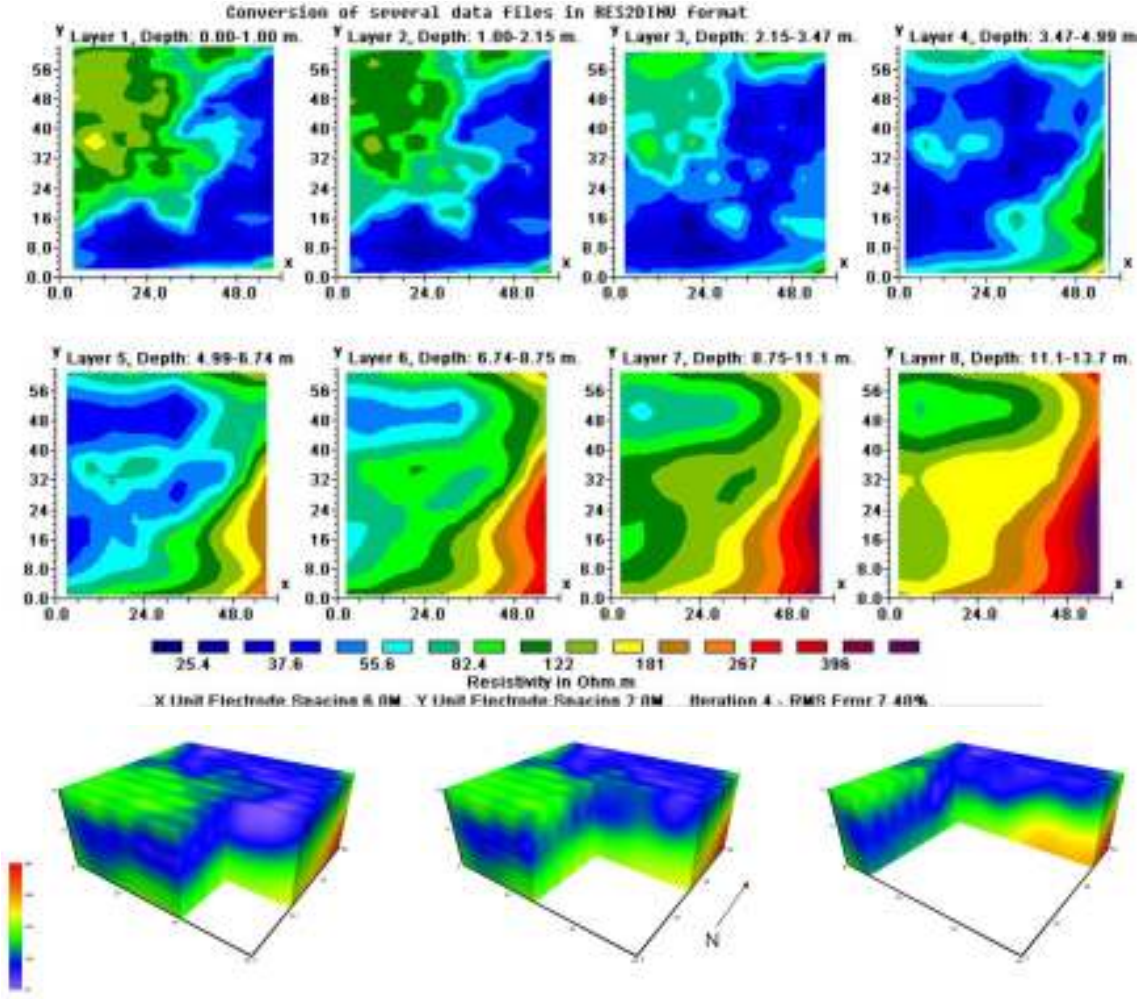

Figure 3.41 –Depth slices of 3D-RES showing the change in resistivity with depth, north follows the x-axis (above) and cube slices showing resistivity variation on vertical profiles (below).

Killiney - Site 3

A resistivity profile with 10 m electrode spacing was recorded in Killiney - Site 3 (Figure 3.42). This dataset was collected close to a borehole record with detailed stratigraphic description, allowing for correlation of resistivity and borehole data. The profile shows three main resistivity signatures (Figure 3.43). Two high resistivity (> 400Ωm) layers along the surface pinching out towards the margins reaching a maximum thickness of 5 m at x-positions 80 – 120 m and 140 – 190 m interpreted as non-saturated soft sediments. This is underlain by a generally continuous layer reaching depths of 20 m below OD dominated by low to medium resistivities (5 - 200Ωm), these sediments are recorded in a borehole located 40 m south (BH-K5) as interstratified sand gravels with clay cobbles and boulders interpreted as saturated soft sediments as recorded in the borehole. A continuous high resistivity layer recorded at depths over 20 m below OD is interpreted as bedrock, which agrees with rock head elevation recorded in BH-K5 at 23.5 m below OD.

Figure 3.42 – Location of Resistivity profile Kil-32-10m and BH-2 recorded in Killiney - Site 1.

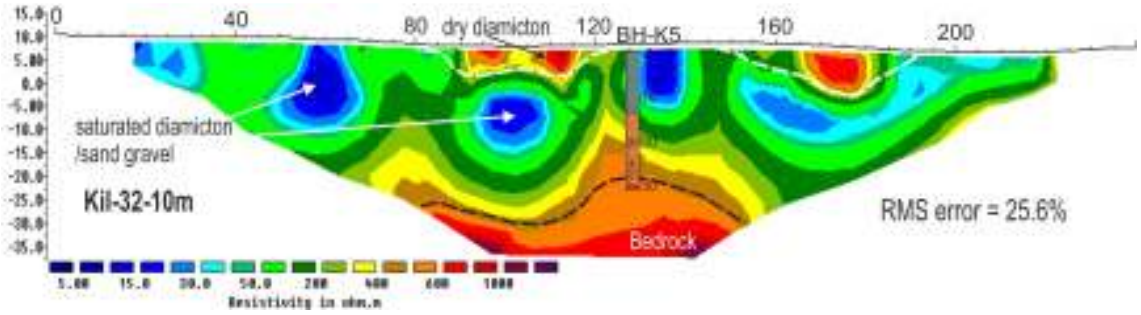

Figure 3.43 – Interpreted resistivity profile Kil-32-10m with an electrode spacing of 10 m.

3.2.2.2.Ground Penetrating Radar

Killiney – Site 1

The GSSI GPR system with a 100 MHz antennae setting was used to collect two radargrams presented as a fence diagram and a 3D cube formeded of 37 profiles with the following dimensions: x-axis = 40 m, y-axis = 30 m and z-axis = 6 m (Figure 3.44).

Figure 3.44 – Location of GPR profiles and 3D Model GPR-3Da collected in Killiney – Site 1.

Radargrams Kil-01 and Kil-02 are presented in Figure 3.45. A few hyperbolae identified in both profiles allowed a sediment calibration velocity of 0.1 m/ns. The radargrams show very poor penetration, no radar signatures are identified in the area below 3 m depth, corresponding with a change in the sediment texture (see sedimentary log 1 in Figure 2 in Rijsdijk et al., 2010) identified on the cliff face. Two moderately continuous reflectors gently dipping west are identified in Kil-01. Kil-02 shows few moderately continuous reflectors dipping south, probably indicating true dip direction towards the southwest.

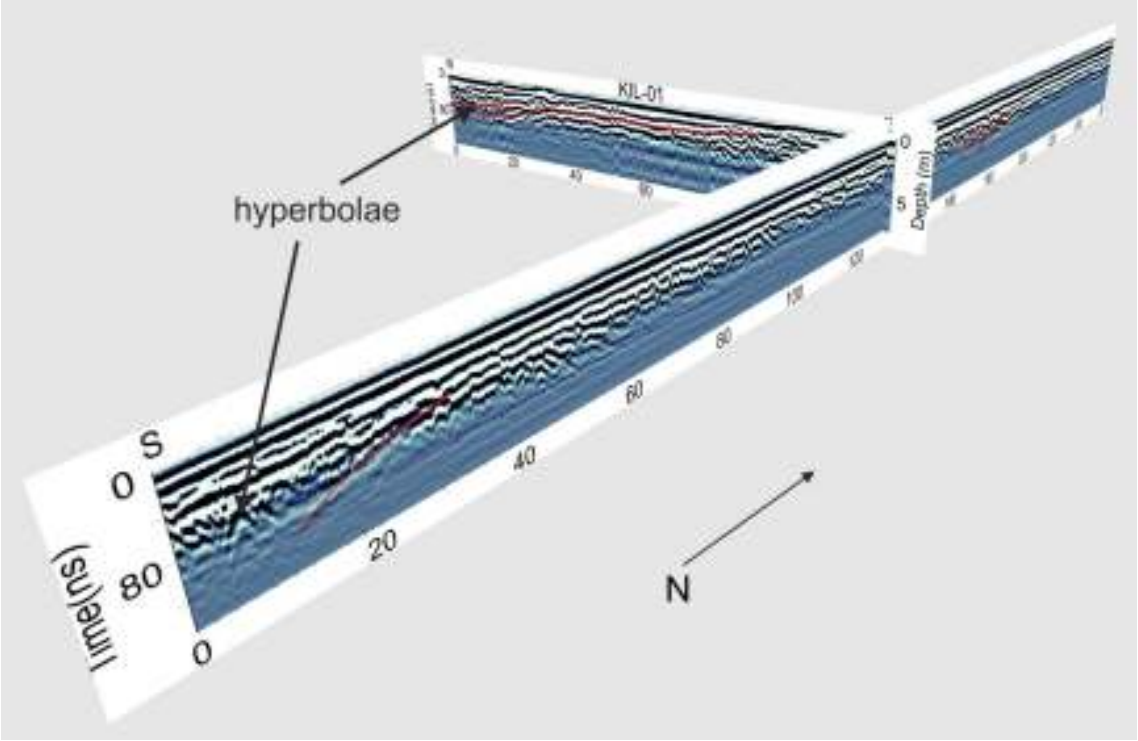

Figure 3.45 – Fence diagram showing GPR profiles Kil-01 and Kil-02 collected in Site 1 using a 100 MHz antennae.

The top four depth slices presented for 3D cube (Figure 3.46) gathered in a relatively depressed region of the coastal plain show very high amplitudes dominating the top four meters of the profile, a sudden change in amplitude is recorded in the 5 m depth slice, corresponding to the lithological change registered in Bh-K3 from gravel to clay dominated sediments (Figure 1.4). The vertical cube slices show few reflectors dipping north in the southwest parts of the cube. However, very little information has been gathered from these datasets.

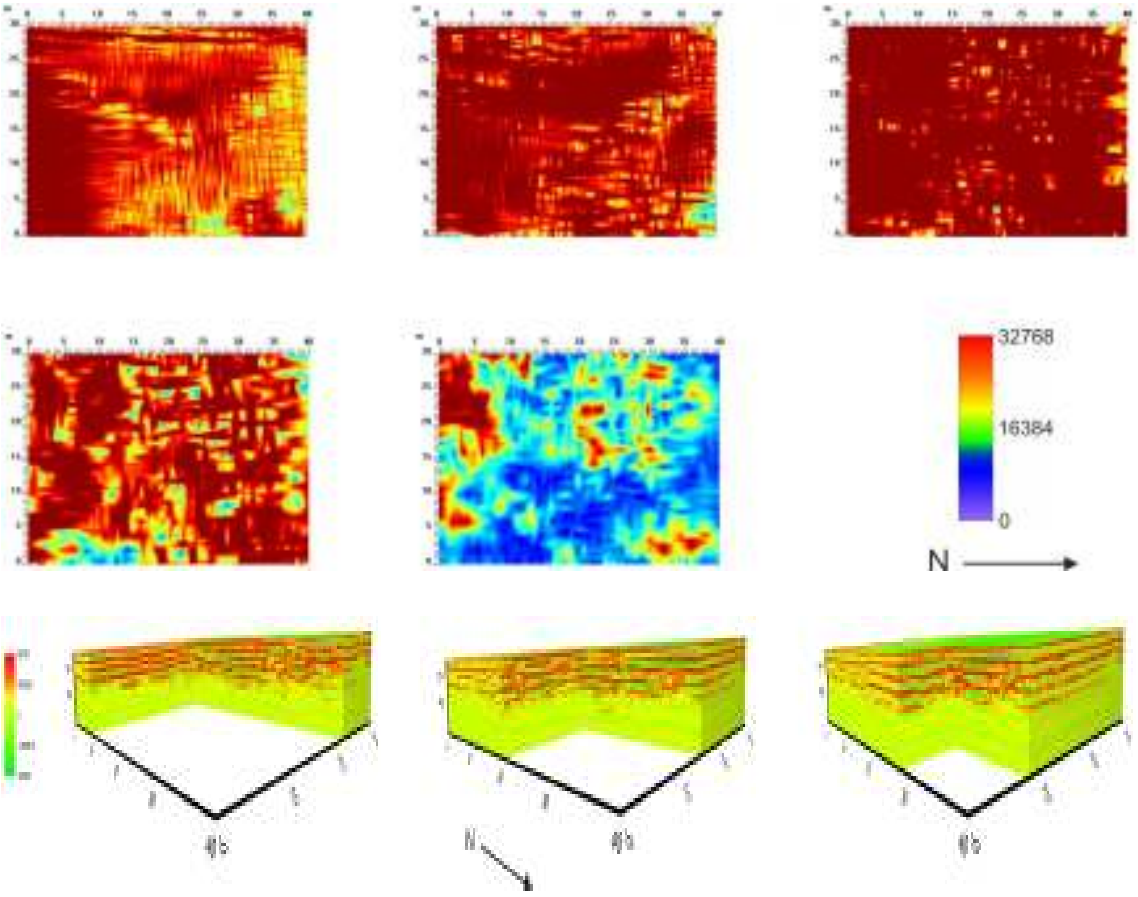

Figure 3.46 – (above) depth slices of GPR-3Da showing the change in amplitude with depth at 1, 2, 3, 4 and 5 m depth and (below) cube slices illustrating resistivity variation on vertical profiles.

Killiney – Site 2

Four radargrams and a 3D cube constituted of 52 profiles with the following dimensions: x-axis = 50 m, y-axis = 50 m and z-axis = 6 m were recorded in this site (Figure 3.47).

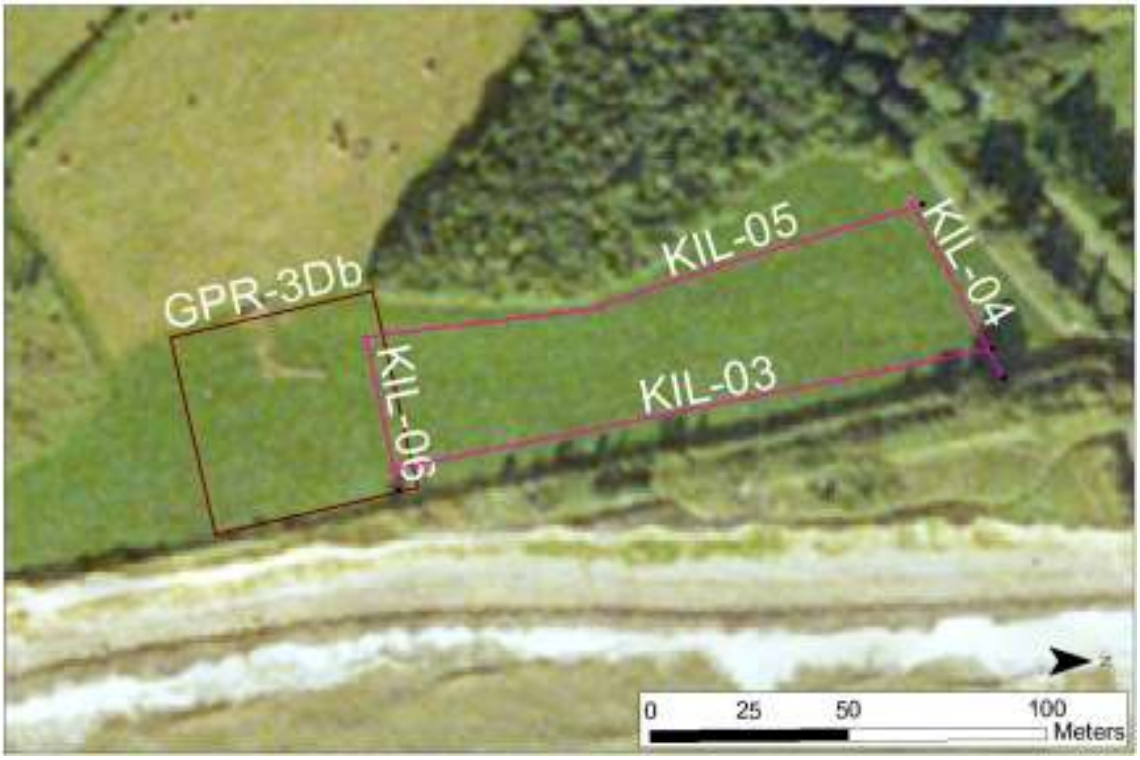

Figure 3.47 – Location of GPR profiles and 3D Model GPR-3Db collected in Killiney – Site 2.

Radargrams Kil-03, 04, 05 and 06 are presented in Figure 3.48. Hyperbolae identified in Kil-03 and Kil-04 allowed a velocity of 0.1 m/ns to be estimated. The radargrams show very poor penetration, no radar signatures are identified in the region below 3 m depth. A change in the sediment texture is identified along the cliff exposure at approximately 3 m from the top (see sedimentary log 23 in Figure 2 in Rijsdijk et al., 2010). Several moderately continuous reflectors gently dipping west identified in Kil-04 and 06 and few further short reflectors dipping south in Kil-03 and 05 are depicted, these probably indicates that true dip direction is towards the southwest.

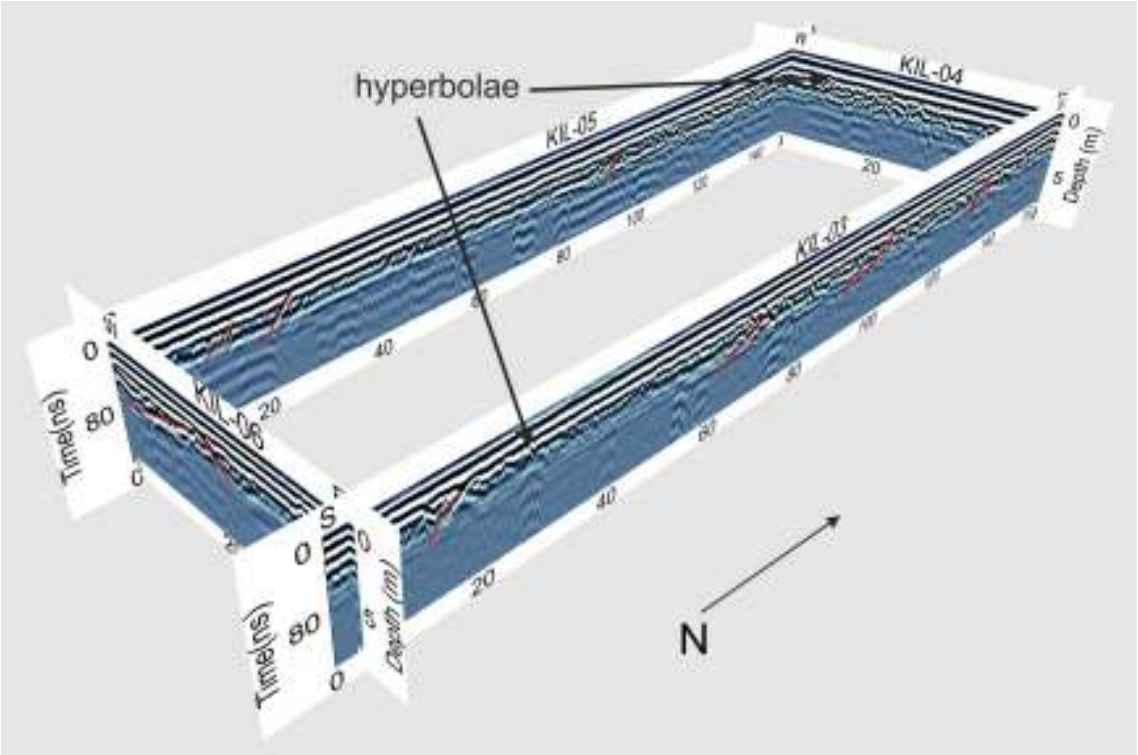

Figure 3.48 – Fence diagram showing GPR profiles collected in Site 2 using a 100 MHz system.

The top three depth slices presented for the 3D cube (Figure 3.49) gathered in the same area where a 3D resistivity model was collected (Figure 3.41) show very high amplitudes dominating the top three meters of the profile, a sudden change in amplitude is recorded in the 4 m depth slice, which corresponds with the sharp sedimentological changes recorded along the cliff face (see sedimentary log 23 in Figure 2 in Rijsdijk et al., 2010). The region below 4 m depth shows higher amplitudes in the southwest parts of the cube, furthermore, reflectors dipping southwestwards are depicted in the vertical cube slices, indicating that the sediments recorded in this area generally dip towards the southwest, , which agrees with the interpretation of the 3D-RES model recorded on the same exact area (Figure 3.41).

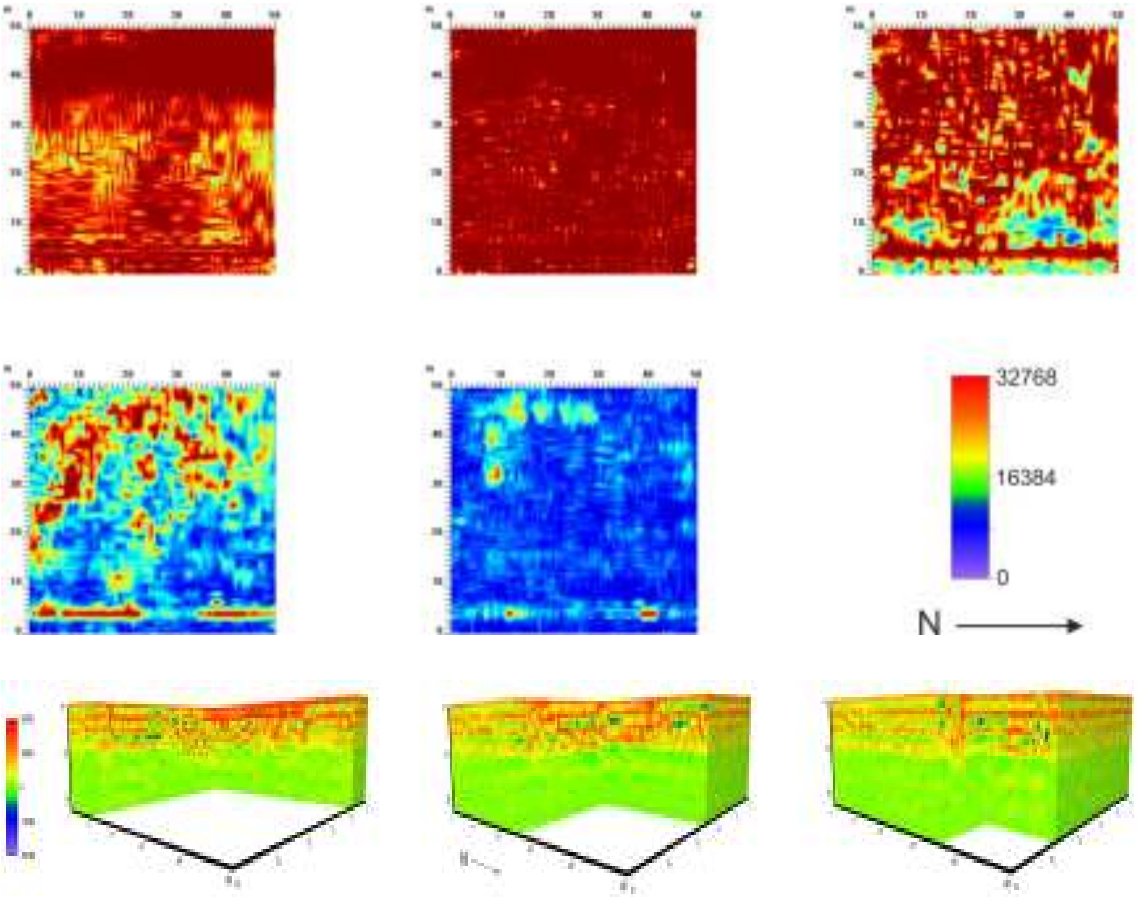

Figure 3.49 – (above) depth slices of GPR-3Db showing the change in amplitude with depth at 1, 2, 3, 4 and 5 m depth and (below) cube slices illustrating resistivity variation on vertical profiles (below).

4. Geomorphology and geophysical data integration

Bull Island and Killiney beach study sites are examples of dynamic coastal environments. The hydrodynamics in the Irish Sea is one of the keys to understanding the coastal processes affecting the two study sites. Hydrodynamics, in the Irish Sea, are mainly dominated by tides. The annual mean dominant flow through the Irish Sea is northward (Elliot et al., 2007). Near the surface water flows parallel to the coast and bottom flows run towards the coast (Gaffney, 2001). These conditions coupled with the coast profile and texture and the existence of man-made structures (i.e. Dublin Port) has contributed to the development of the current coastline.

Bull Island is currently undergoing depositional processes involving significant accretion in the southern parts of the island, two buildings located 250 m and 100 m from the current coastline, representing the coast position during 1916 and 1971 (Figure 3.1), respectively, allow a coastal progradation estimation during the last century of ca. 2.4 m/year in the south region of the island. On the other hand, the coastal profile on the north-eastern parts of Bull Island has sustained slower coastal progradation, estimated from Harris (1977) at ca. 0.55 m/year and some parts of the coastline are currently enduring erosional processes (Figure 3.22). Killiney beach is affected by erosional processes that forced shifting westwards the railway line connecting Dublin and Bray, the coastal erosion of the cliff has been estimated at ca. 25 m since 1903 (Rijsdijk et al., 2010), thus ca. 0.23 m/year. The generally straight cliff profile (Figure 3.2) shows points slightly protruding from it, which coincide with areas where sea erosion defences have been built, which are probably causing further erosion in non-defended parts of the coast. Geophysical characterization combined with geomorphology mapping and borehole records allowed the internal architecture of the sediments in both study sites to be characterized.

ERT data collected in Bull Island allowed an estimation of the depth to bedrock in the area, the position of the interface between salt and freshwater aquifers and the thickness of unsaturated sediments to be made. Four main resistivity signatures were depicted in Bull Island. Sand dunes dominating the higher ground areas present resistivity values over 400 Ωm. Low to medium resistivities recorded at the surface on fresh water marsh deposits and at depth in the sand dunes areas correspond with fresh water shallow aquifer associated with the sand dune complex. Saline aquifer domain is depicted as a

generally continuous layer with resistivity values below 30 Ωm recorded at depths in the sand dunes region and at the surface in the areas dominated by beach deposits and salt marsh. Medium resistivity layers underlying the saline domain are interpreted as bedrock at depths of 15 – 25 m below OD in Site 1, 28 – 35 m below OD in Site 2 and 14 - 17 m below OD in Site 3, indicating lower rock head in the central and northern parts of the Island and concurring reasonably with depth to bedrock recorded in borehole records recorded in Dublin Port and Howth Peninsula (Figure 1.4). Finally, a number of artefacts showing relatively high resistivities (> 200 Ωm) within the saline domain region (<30 Ωm) are depicted in some of the ERT profiles (Figures 3.4, 3.9, 3.10, 3.16). These may be associated with anthropogenic features, e.g. shipwrecks. Over 140 historical shipwreck events are recorded in the Dublin Bay (http://www.irishwrecksonline.net/), however, further research should be conducted in order to confirm the artefacts as such.

GPR has been widely used in the characterization of the internal architecture of sand dune deposits (e.g. Bristow et al., 2000; Neal et al; 2002; Clemensen et al., 2007). The internal structure of coastal dunes is strongly conditioned with dune type, vegetation, orientation with respect to the prevailing wind and orientation with respect to the coastline (Bristow et al., 2000). Bull Island coast has a meso- to macrotidal regime with dominant waves from the southeast and prevailing southwest wind (Elliot et al., 2007). Sand dunes in Bull Island are generally longitudinal parallel to the coastline breaking up in the island middle region into discontinuous hummocks with ridge crest accumulation; these changes are usually caused by an increase of sand mobility associated with increasing winds or decreasing vegetation cover (Short and Hesp, 1982). The intense use of the island as an amenity by the Dublin residents may have reduced vegetation cover in the areas closer to the car parks located, therefore, the modifications observed in the dune morphology of the in the island middle region may be associated with vegetation changes propitiated by urban pressure. The sand dunes gradually increase their size from south to north, the rapid coastal progradation in the south-western parts of the island does not permit sediment supply to the dunes located landward, thus not allowing for their vertical growth. Dune ridge development is associated with coastal progradation while dunes are eroded during storms, thus a stable coast is established providing more time for dune development and resulting in higher foredune ridges (Bristow et al., 2000).

Seven different radar facies are recognized on the basis of reflection character and geometry: Most of the dunes are composed of foreslope and rearslope accretion deposits, the slacks between slopes are either composed of interstratified foreslope and rear-slope deposits and/or bio-topographic accumulation deposits. Foreslope deposits are characterized by moderately continuous subparallel gently seaward dipping reflectors, some of these present a continuous reflector dipping southeast showing continuity under the water table illustrating the former coastline; rearslope accretion deposits are defined by discontinuous sinuous oblique shingled reflectors and bio-topographic accumulation is illustrated by low amplitude discontinuous sinuous concave and convex-up reflectors. Embryonic dunes are recorded along the seaward side of the foredunes system for 2.5 Km from Dublin Port North Wall and are characterized by high amplitude continuous reflector combined with scattered oblique chaotic reflectors. Large freshwater marshes dominating the southern interdune region gradually tailing off north-eastwards are characterized by high amplitude continuous horizontal reflectors. Salt marsh is also defined by high amplitude continuous horizontal reflectors. Marine sediments consisting of continuous seaward gently dipping moderately continuous reflectors mostly developing beneath the water-table underlain all the deposits described. Finally, man-made ground consisting of dams built to protect the fresh water marshes and golf links from seawater flooding are characterized by chaotic reflectors.

The setting recorded in Killiney beach study site consisting of soft cliffed coast is recorded all along the Irish east coast, especially in Counties Wexford and Wicklow where intense coastal erosion is also prevalent (RPS, 2007). ERT data collected in Killiney allowed the rock head elevation in the area to be estimated and the spatial distribution of soft sediments overlying it, providing further information for future remedial actions potentially taken on these areas. Medium resistivities along the surface (200 - 500 Ωm) are associated with sand and gravel deposits described along the cliff by Rijsdijk et al. (2010). Low-medium resistivity values (100 Ωm) with lenses showing low resistivities (<40 Ωm) are described along the cliff as clast rich silty diamicton (Rijsdijk et al., 2010) showing seepage in some locations, which may be associated with the lower resistivities. High resistivity values (>600 Ωm) recorded along the lower regions of all the resistivity profiles are interpreted as bedrock. These high resistivity areas show sudden lateral changes to low-medium resistivities, which may relate to the

nature of metamorphic rocks (gneiss and schist) underlying the area. The pattern is repeated on the profiles orientated south-north (Figures 3.37 and 3.38), whereas profiles collected west-east show rock head level as a continuous sharp contact (Figure 3.39 and 3.43). Rock head elevation is estimated from borehole and geophysical data at 10 m below OD in the profiles recorded in the western margin of the Killiney area and gradually slopping down to maximums of 24 m below OD in the region closer to the coastline (Figure 3.39). Variations from north to south in rock head elevation are not substantial, indicating that the coastal plain soft sediments deposited on bedrock with a flat profile from north to south and gradually sloping down towards the east from west to east.

GPR surveys carried out in Killiney beach area provided limited results. The lithological composition of the sediments (high silts and clays content) did not allow for deep penetration of the GPR electromagnetic waves. Hyperbolae reflections allowed calibrating sediments velocity at 0.1 m/ns. Changes in lithology recorded in boreholes and along the cliff face correspond with sudden signal-loss depicted in the radargrams at approximately 3 m depth. Few moderately continuous reflectors and in the 3D cube dataset gathered in Site 2 indicate the true dip direction of the sediments in the area towards the southwest. However, information gathered from these datasets was rather poor.

5. Summary and further research

Geomorphological mapping and 3D geophysical characterization in County Dublin allowed a depiction of the main stratigraphic and hydrostratigraphic units of two study areas, one encompassing coastal sedimentary processes and the other undergoing erosional processes.

ERT data allowed the depth to bedrock in both areas to be estimated and and delineation of the spatial distribution of soft sediments in Killiney and the hydrostratigraphic units in Bull Island. These data provide extra information for future remedial actions related with sea level change potentially taken on urban areas.

GPR data proved to be an excellent tool for depicting the internal architecture of sand dune deposits, the display of the data as 2.5D fence diagrams improved the knowledge on the genesis and evolution of the Island. However, this method performed quite

poorly in the Killiney study site. The lithological composition of the sediments with high silt and clay content did not allow for deep penetration of the electromagnetic waves and thus did not allow for the identification of radar facies.

Further research using other geophysical methods could possibly compensate for this drawback. The use of seismic refraction and reflection surveys along the Killiney and Bull island study sites would help confirm the rock head elevation presented in this work.

6. Methodological evaluation of bathymetry extraction using remote sensing

Introduction

Coastlines are in continuous change largely affected by human activity, and effects of climate change such as sea level rise, extreme climate etc. For this an evaluation of the effectiveness of precise water depth estimation in shallow waters is extremely important.

The main objective of this research is to evaluate the effectiveness of high spatial and spectral resolution of the new imagery data on water depth measurements using an empiric regression bathymetric model obtained from passive remote sensing.

Review of bathymetric inversion methods

The main principle underlying the retrieval of bathymetric information from optical remote sensing images is that when light passes through water it becomes attenuated by interaction with the water column. Different bands will have different attenuation and penetration properties depending on the part of the spectrum.

The bathymetric approaches involving satellite imagery data are regarded as a fast and economically advantageous solution to automatic water depth calculation in shallow waters (Stumpf et al., 2003; H. Su et al., 2008).

The feasibility of deriving bathymetric estimates from remote sensing imagery was first demonstrated using aerial photographs over clear shallow water (Lyzenga 1978). Since then a wide variety of empirical models has been proposed and evaluated for bathymetric estimations by establishing the statistical relationship between image pixel values and field-measured water depth values.

The most popular approach was proposed by Lyzenga (1978, 1981, 1985) and was based on the fact that the bottom-reflected reflectance is approximately a linear function of the bottom reflectance and an exponential function of the water depth. Stumpf et al. (2003) presented an algorithm using a ratio of reflectance and demonstrated its benefits to retrieve depths from IKONOS imagery even in deep water (>25m) contrary to standard linear transform algorithms. Jupp (1988) introduced an algorithm for determining the depth of penetration (DOP) zones for every band and then for calibrating depths within DOP zones. This method has recently successfully been applied to high resolution Worldview and IKONOS images by Deidda and Shanna (2012) and Su et al., (2008) respectively through IDL modules implemented in ENVI

software. The technique has been expanded to include the use of passive optical multi-spectral satellite imagery including Landsat (Benny and Dawson 1983; Jupp et al. 1985; Lyzenga 1981; 1985), QuickBird (Mishra et al. 2006; Conger et al. 2006) images (Su et al., 2008) and from SPOT images in shallow waters (Lafon et al., 2002, Liu, et al., 2010).

Data

Several datasets would be required to implement this methodology in the Irish context.

Elevation Datasets

- LiDAR OSi (2009): Point source data collected in 2009 by the Ordnance Survey.
- OPW LIDAR (2006) survey digital datasets: Lidar point data with a spatial resolution of approximately 1m collected by the Office of Public Works.
- Offshore INFOMAR Multibeam bathymetry 2010-2011 (GSI-Marine Institute).

Satellite Data

- Multispectral SPOT 5 (colour 2.5, 5 and 10m) for 2010 and 2011 obtained for the Dublin area.

Scene ID: 501842211030111594 42V

Scene ID technical Charact	501842211030111594 42V		
Product	2.5 m C		
Satellite	Spot5		
Acquisition date DATEdate	2011-03-01 MARMARC		
Acquisition time	11:59:44		
Gains			
Cloud cover rating	ABAAAAAA		
Snow cover rating	00		
Angle of incidence	25.98		
Shift of scene along the track	0		
	Geographic location of scene		
Latitude of centre	53.19°		
Longitude of centre	-5.72°		
Latitude of NW corner corner	53.56		
Longitude of NW corner	-6.07		
Latitude of NE corner	53.32°		
Longitude of NE corner	-5.05		
Latitude of SW corner	53.05°		
Longitude of SW corner	-6.40°		
Latitude of SE corner	52.82°		
Longitude of SE corner	-5.38°		
Radiometric information	Spectral bands in quicklook:3		
	Saturated	Adapt. Min	Adapt. Max thres
Band 1	0.10%	56	82

Band 2	0.10%	33	80
Band 3	0.10%	12	

Scene ID: 501724109060111122512J

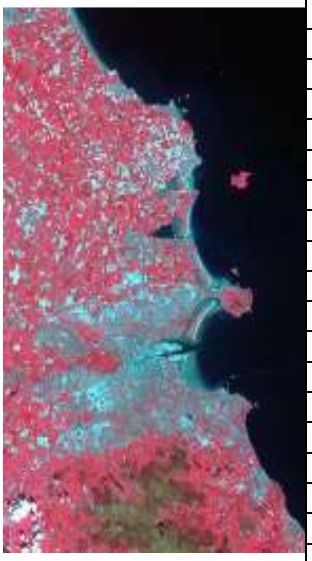

Scene ID technical Charact	501724109060111122512J		
Product	10 m C		
Satellite	Spot5		
Acquisition date DATEdate	2009-06-01 or 01/06/2009		
Acquisition time	11:22:51		
Gains	7735		
Cloud cover rating	AAAABBBB		
Snow cover rating	0000		
Angle of incidence	-15.04°		
Shift of scene along the track	4		
	Geographic location of scene		
Latitude of centre	53.45°		
Longitude of centre	-6.39°		
Latitude of NW corner corner	53.78°		
Longitude of NW corner	-6.74°		
Latitude of NE corner	53.63°		
Longitude of NE corner	-5.80°		
Latitude of SW corner	53.26°		
Longitude of SW corner	-6.96°		
Latitude of SE corner	53.11°		
Longitude of SE corner	-6.03°		
Radiometric information	Spectral bands in quicklook:4		
	Saturate	**Adapt. Min**	**Adapt. Max thres**
Band 1	0%	55	148
Band 2	0%	31	174
Band 3	0%	5	146
SWIR	0%	4	189

Scene ID: 501824209091211443l2U

Scene ID technical Charact	501824209091211443l2U		
Product	5 m C		
Satellite	Spot5		
Acquisition date DATEdate	2009-09-12		
Acquisition time	11:44:31		
Gains			
Cloud cover rating	ABAAABBB		
Snow cover rating	00000000		
Angle of incidence	9.29°		
Shift of scene along the track	0		
	Geographic location of scene		
Latitude of centre	53.19°		
Longitude of centre	6.40°		
Latitude of NW corner corner	53.53°		
Longitude of NW corner	-6.70°		
Latitude of NE corner	53.36°		
Longitude of NE corner	-5.83°		
Latitude of SW corner	53.02°		
Longitude of SW corner	-6.98°		
Latitude of SE corner	52.84°		
Longitude of SE corner	6.12°		
Radiometric information	Spectral bands in quicklook:3		
	Saturated pixels	**Adapt. Min**	**Adapt. Max thres**
Band 1	0%	74	131
Band 2	0%	5311	153
Band 3	0%		

Methodology

The methodology indicated here has some similarities to that introduced by Jupp et al. (1985) for bathymetry extraction. ArcGIS 10 and ENVI packages would be used in order to pre-process and to execute the corrections needed.

Pre-processing

- Ground truthing data: LIDAR point source data files (OSi, 2009; OPW, 2006) w downloaded and projected into UTM29N and imported into a file geodatabase.
- Check training sites: Before applying logarithms the data from the two multi-spectral images examined to explore the relationship between observed reflectance and water depth.
- Rectification (Geometrically and geographically): where many ground control or reference points exist.
- Atmospheric correction applied to correct for the atmospheric effects.

- The sunglint effects corrected (Hedley et al. 2005) taking in account whether an atmospheric correction has been applied or not.
- A depth-invariant image for water colum correction to be obtained (Lyzenga 1978, 1981; Green et al., 2000].);
- An unsupervised classification performed on the two depth-invariant scenes, producing classes of homogeneous sea bottom, of which the one corresponding to sand is selected.

Depth model extraction

- Determine the Depth Of Penetration (DOP) zones calculated for the selected sand bottom class using Log Ratio Transform, Principal Components, and Independent Components or the Jupp method (Jupp, 1988). Calibrate the model using our ground truth data and calculate depth values.
- Validation performed to evaluate the accuracy of the model the surveyed depth values and the calculated ones for several calibration areas.

Future work

Current INFOMAR multibeam bathymetry gaps filled with these data and the procedure extended to adjacent areas and integrated with multiple coastal datasets.

7. References for Geophysics component of research

Ballantyne, C. K., McCarroll, D., Stone, J. O. 2006. Vertical dimensions and age of the Wicklow Mountains ice dome, eastern Ireland, and implications for the extent of the last Irish Ice Sheet. Quaternary Science Reviews 25, 2048–2058.

Bowen, D. Q. 1973. The Pleistocene succession of the Irish Sea. Proceedings of theGeologists' Association 84, 249–272.

Bristow, C. S., Chroston, P. N., Bailey, S. D. 2000. The structure and development of foredunes on a locally prograding coast: insights from ground-penetrating radarsurveys, Norfolk, UK. Sedimentology, 47, 923-944.

Caloca, S. 2006. Geophysical investigation of Quaternary glacial sediments in South Co. Westmeath and North Co. Offaly. Unpublished Master thesis, EnvironmentalGeophysics Unit, NUI Maynooth.

Carter, R.W.G. 1991. Effects of climate change on the coastline of Ireland. Unpublished report to the Irish Government as part of the ―Climate Change and its impact on Ireland programme.

Clemmensen L. B., Bjørnsen, M., Murray, A., Pedersen, K. 2007. Formation of aeolian dunes on Anholt, Denmark since AD 1560:A record of deforestation and increased storminess. Sedimentary Geology 199, 171–187.

Comas, X., Slater, L., Reeve, A. 2004. Geophysical evidence for peat basin morphologyand stratigraphic controls on vegetation observed in a northern peatland. Journalof Hydrology 295, 173–184.

Devaney, F. H. 2008. The Alder Marsh: Ecohydrology and Restoration Prospects of a Desiccating Dune Slack. Ph.D. thesis, University College Dublin.

Doetsch, J., Linde, N., Pessognelli, M., Green, A. G., Günther, T., 2011. Constraining 3-D electricalresistance tomography with GPR reflection data for improved aquifer characterization.Journal of Applied Geophysics. doi:10.1016/j.jappgeo.2011.04.008.

Elliot, A., Hartnett, M., O'Riain, G., Dollard, B. 2007. PRISM project: Predictive Irish Sea Models. European Union Interreg IIIA. Dublin.

Eyles, N., McCabe, A. M., 1989a. Glacimarine facies within subglacial tunnel valleys:the sedimentary record of glacioisostatic downwarping in the Irish Sea Basin.Sedimentology 36, 431–448.

Eyles, N., McCabe, A. M., 1989b. The Late Devensian (<22,000 BP) Irish Sea Basin: thesedimentary record of a collapsed ice sheet margin. Quaternary ScienceReviews 8, 307–351.

Farrell E. R., Coxon, P., Doff D. H. ,Priedhomme, L. 1995.The genesis of brown boulder clay of Dublin.Quarterly Journal of Engineering Geology, 28.

Gaffney, S. P. 2001. Use of satellite imaginary to assess trends in water clarity in theIrish Sea. Ph. D thesis, National University of Ireland, Galway, Galway, Ireland, pp.205.

Hoare, P. G. 1975. The pattern of glaciation in county Dublin. Proceedings of the Royal Irish Academy 75B, 207–224.

Harris, C. R. 1977. Sedimentology and Geomorphology in: The North Bull Island, Dublin Bay, a modern coastal natural history, ed. D. W. Jeffrey. The Royal Dublin Society. Dublin.

IPCC, 2007. Climate Change 2007: impacts, adaptation. Contribution of Working Group II to the Fourth Assessment Report of the Intergovernmental Panel on Climate Change. Cambridge University Press, Cambridge, United Kingdom and New York, NY, USA.

Jol, H. M. and Bristow, C. J. 2003. GPR in Sediments: advice on data collection, basicprocessing and interpretation, a good practice guide. Pp. 9-29 in Bristow, C. J. AndJol, H.M. (Eds) Ground Penetrating Radar in Sediments, The Geological Society,London.

McConnell, B., Philcox, M. E., Sleeman, A. G., Stanley, G., Flegg, A. M., Daly, E. P., Warren, W. P. 1994. A Geological Description to Accompany the BedrockGeology 1:100,000 Map Series, Sheet 16, Kildare – Wicklow. GeologicalSurvey of Ireland, Dublin, 69 pp. þ 1:100,000 scale Bedrock Geology Map,sheet 16.

McFadden, L., Nicholls, R. J, Penning-Roswell, E. 2007. Managing coastal vulnerability. Elsevier, Amsterdam, pp 261.

McLaughlin, S. 2001. Assessment and Development of a Coastal Vulnerability Index for Northern Ireland Employing GIS Techniques. Unpublished D.Phil. Thesis, University of Ulster, Coleraine.

Mitchell, G. F., Penny, L. F., Shotton, F. W.,West, R. G. 1973. A correlation of Quaternarydeposits in the British Isles. Geological Society of London Special Report 4.

Mulrennan, M. E. 1990. The Geomorphic Development of the Barrier-Beach Complexes of the North County Dublin Coastline. Unpubl. Ph.D. thesis. University College Dublin, 2 vols.

Mulrennan, M. E. 1993. Changes since the Nineteenth Century to the Estuary-Barrier Complexesof North County Dublin. Irish Geography, 26: 1, 1 — 13.

Neal, A. 2004. Ground Penetrating Radar and its use in sedimentology: principles,problems and progress. Earth-Science Reviews 66, 261–330.

Neal, A., Richards, J., Pye, K., 2002. Structure and development of shell cheniers inEssex, southeast England, investigated using high-frequency ground-penetratingradar. Marine Geology 185, 435–469.

Pellicer, X. M. 2008. Quaternary Geology of County Dublin: a description to accompany the Quaternary Geology Map of County Dublin. Unpublished report. Geological Survey of Ireland.

Pellicer, X. M., 2010, Geophysical Characterisation and Evolutionary Model of the Quaternarysediments in the North Offaly region of Central Ireland. Unpublished Ph.D Thesis, Department of Geography, National University of Ireland, Maynooth.

Rijsdijk, K. F., Warren, W. P., van der Meer, J. J. M. 2010. The glacial sequence at Killiney, SE Ireland: terrestrial deglaciationand polyphase glacitectonic deformation. Quaternary Science Reviews, 29, 696–719.

Robinson, A. 2009. An investigation of coastal erosion retreat boundaries of the East Coast of Ireland between 1864 and 2009 and development of a volumetric change detection methodology to model the spatial extents of two surface grids using lidar and RTK GPS data sets." Unpublished thesis. Department of Geography. NUIM.

RPS, 2007. The Murrough, Co. Wicklow coastal protection study. Wicklow County Council. Doc num. IBE0055/SG/Aug 07.

Sharples, C. 2006. Indicative Mapping of Tasmanian Coastal Vulnerability to Climate Change and Sea Level Rise: Explanatory Report. Report to Department of Primary Industries, Water & Environment, Tasmania, 2nd Edition, pl.

Sensors and Software.2001. Ekko for DVL, Pulse Ekko 100. User's guide Version1.0. Sensors and Software. Ontario.

Sensors and Software. 2003 Ekko View Enhance and deLuxe, User's guide. Sensorsand Software. Ontario.

Short, A. D., Hesp, P. A. 1982. Wave beach and dune interactionsin southeastern Australia. Mar. Geol., 48, 259±284.

Slater, L., Reeve, A. 2002. Understanding peatland hydrology and stratigraphy using integratedelectrical geophysics. Geophysics 67, 365–378.

Synge, F. M., 1963. A correlation between the drift of south-east Ireland and those ofwest Wales. Irish Geography 5, 73–82.

Synge, F. M., 1977. The coasts of Leinster (Ireland). In: Kidson, C., Tooley, M.J. (Eds.), The Quaternary History of the Irish Sea. Geological Journal Special Issue, vol. 7. Seel House Press, Liverpool, pp. 115–131.

Trafford, A., 2009. Mapping thickness of raised peat bog deposits using GPR. Near Surface2009 — 15th European Meeting of Environmental and Engineering Geophysics,Dublin, Ireland.

Vanneste, K., Verbeeck, K., Petermans, T., 2008. Pseudo-3D imaging of a low-sliprate,active normal fault using shallow geophysical methods; the Geleen Fault in theBelgian Maas River valley. Geophysics 73 (1), B1–B9.

Warren, W. P., 1985. Stratigraphy. In: Edwards, K. J., Warren, W. P. (Eds.), The Quaternary History of Ireland. Academic Press, London, pp. 39–65.

Warren, W. P, 1991. Ireland 1991: field guide for excursion. Dublin, INQUA Commission on Formation and properties of glacial deposits.

8. References for Remote Sensing component of research

Benny, A. H.; Dawson, G. J. 2983. Satellite imagery as Aid to Bathymetric Charting in the Red. Cartographic Journal, The, Volume 20, Number 1, June 1983 , pp. 5-16(12)

Conger, C. L., E. J. Hochberg, C. H. Fletcher, and M. J. Atkinson. 2006. Decorrelating remote sensing color bands from bathymetry in optically shallow waters. IEEE transactions on Geoscience andRemote Sensing 44:1655–1660.

Deidda, M. and Sanna, G . 2012. Bathymetry extraction uisng Wolrdview high resolution images. International Archives of the Photogrammetry, Remote Sensing and Spatial Information Sciences, Volume XXXIX-B8, 2012 XXII ISPRS Congress, 25 August – 01 September 2012, Melbourne, Australia. Abstract.

Deidda, M and and Sanna, G.2012. Pre-processing of high resolution satellite images for sea bottom classification. Italian Journal of Remote Sensing - 2012, 44 (1): 83-95doi: 10.5721/ItJRS20124417.

Green E.P., Mumby A.J., Clark E., Clark C.D. (2000) - Remote Sensing Handbook for Tropical Coastal Management. UNESCO Publishing, Paris.

Hedley J.D., Harborne A.R., Mumby P. J. (2005) - Simple and robust removal of sun glint for mapping shallow water benthos. International Journal of Remote Sensing,10: 2107-2112. doi: http://dx.doi.org/10.1080/0143116050003408.)

Jupp, D. L. B. 1989. Background and extension to depth of penetration(DOP) mapping in shallow coastal waters. Conference on Remote Sensing Application Projects Using microBRIAN Image Processing System.

Jupp, D. L. B., K. K. Mayo, D. A. Kuchler, D. V. R. Claasen, R. A. Kenchington, and P. R.Guerin. 1985. Remote sensing for planning and managing the great Barrier Reef of Australia. Photogrammetria 40:21–42.

Jupp, D.L.B., 1988, Background and extensions to depth of penetration (DOP) mapping in shallow coastal waters. Proceedings of the Symposium on Remote Sensing of the Coastal Zone, Gold Coast, Queensland, September 1988, IV.2.1-IV.2.19Lafon, Virginie, et al. "Determining ridge and runnel longshore migration rate using spot imagery." *Oceanologica Acta* 25.3 (2002): 149-158.

Liu, Shanwei, Jie Zhang, and Yi Ma. (2010). Bathymetric ability of SPOT-5 multi-spectral image in shallow coastal water. *Geoinformatics, 2010 18th International Conference on*. IEEE, 2010.

Lyzenga, D. R. 1978. Passive remote sensing techniques for mapping water depth and bottom features. Applied Optics 17:379–383.

Lyzenga, D. R. 1981. Remote sensing of bottom reflectance and water attenuation parameters in shallow water using aircraft and Landsat data. International Journal of Remote Sensing 2:71–82.

Lyzenga, D. R. 1985. Shallow-water bathymetry using combined lidar and passive multispectral scanner data. International Journal of Remote Sensing 6:115–125.

Mishra, D., S. Narumalani, D. Rundqulst, and M. Lawson. 2006. Benthic habitat mapping in tropical marine environments using QuickBird multispectral data. Photogrammetric Engineering &Remote Sensing 72:1037–1048.

Stumpf, Richard P., Kristine Holderied, and Mark Sinclair.2003. "Determination of water depth with high-resolution satellite imagery over variable bottom types."*Limnology and Oceanography* (2003): 547-556..

Su, H., Liu, H., Heyman, W. D. 2008. Automated Derivation of Bathymetric Information from Multi-Spectral Satellite Imagery Using a Non-Linear Inversion Model. Marine Geodesy Vol. 31, Iss. 4, 2008.

Appendix

BULL ISLAND- SITE 1

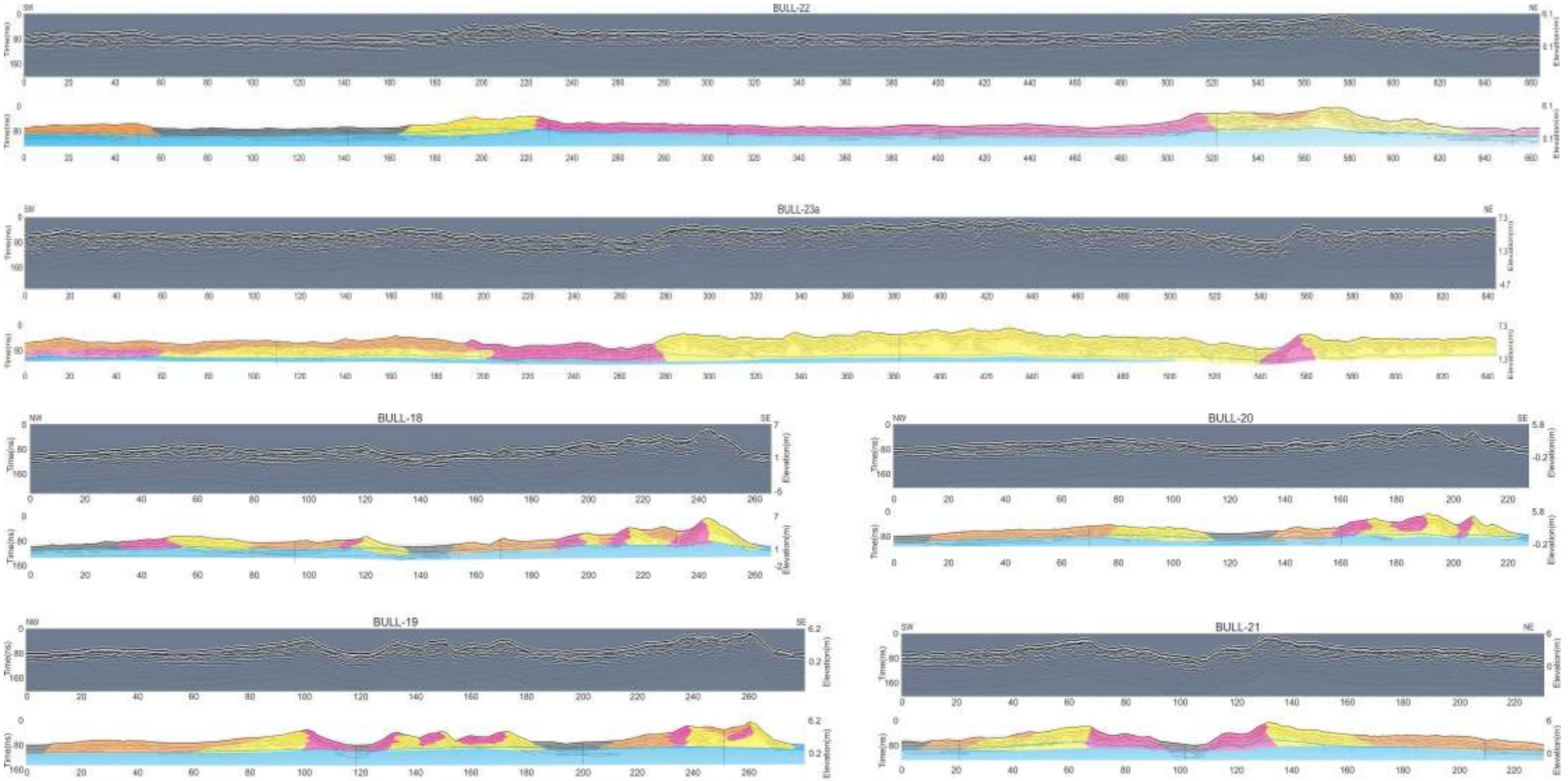

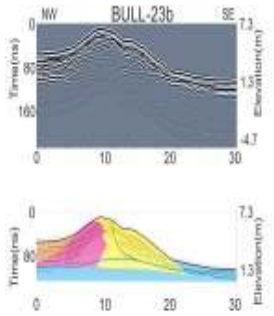
NW
BULL-23b
SE
Time(ns)
Elevation(m)

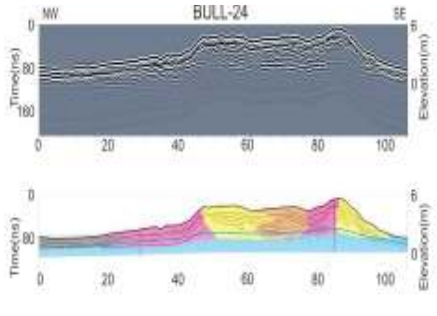
NW
BULL-24
SE
Time(ns)
Elevation(m)

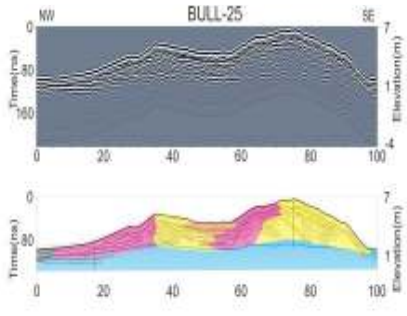
NW
BULL-25
SE
Time(ns)
Elevation(m)

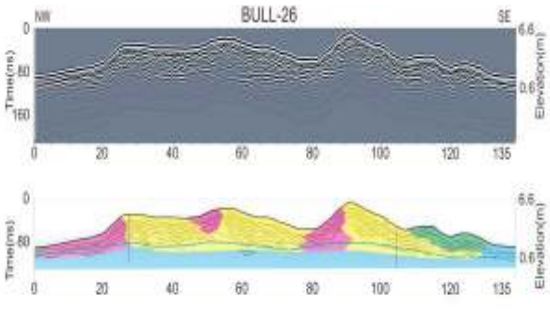
NW
BULL-26
SE
Time(ns)
Elevation(m)

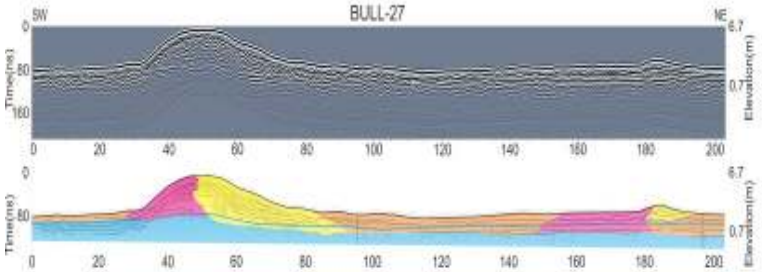
SW
BULL-27
NE
Time(ns)
Elevation(m)

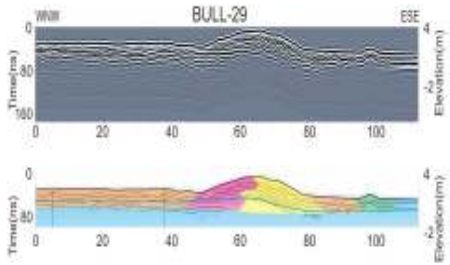
WNW
BULL-29
ESE
Time(ns)
Elevation(m)

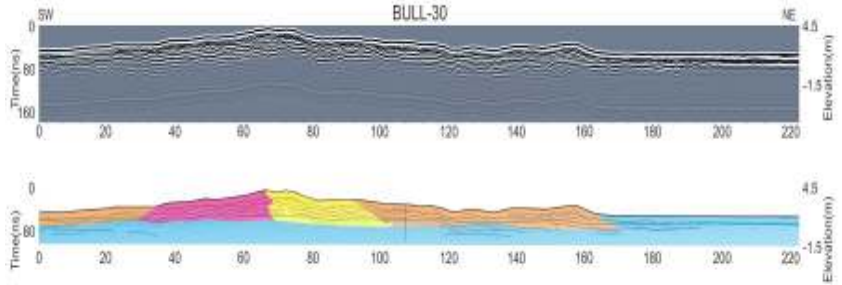
SW
BULL-30
NE
Time(ns)
Elevation(m)

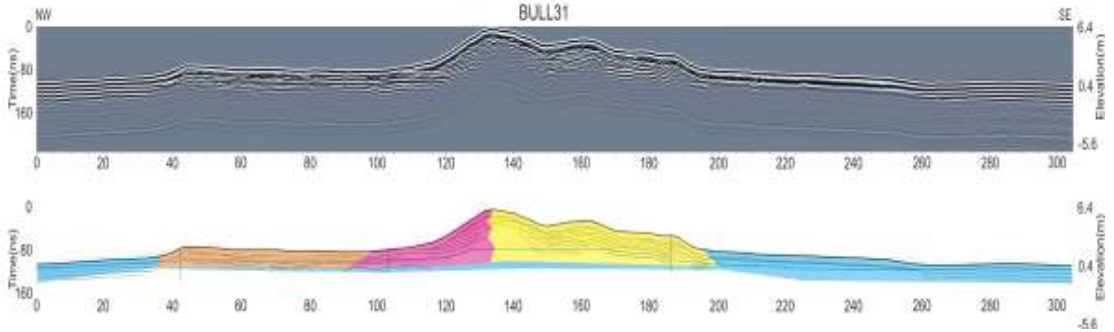
NW
BULL31
SE
Time(ns)
Elevation(m)

BULL ISLAND - SITE 2

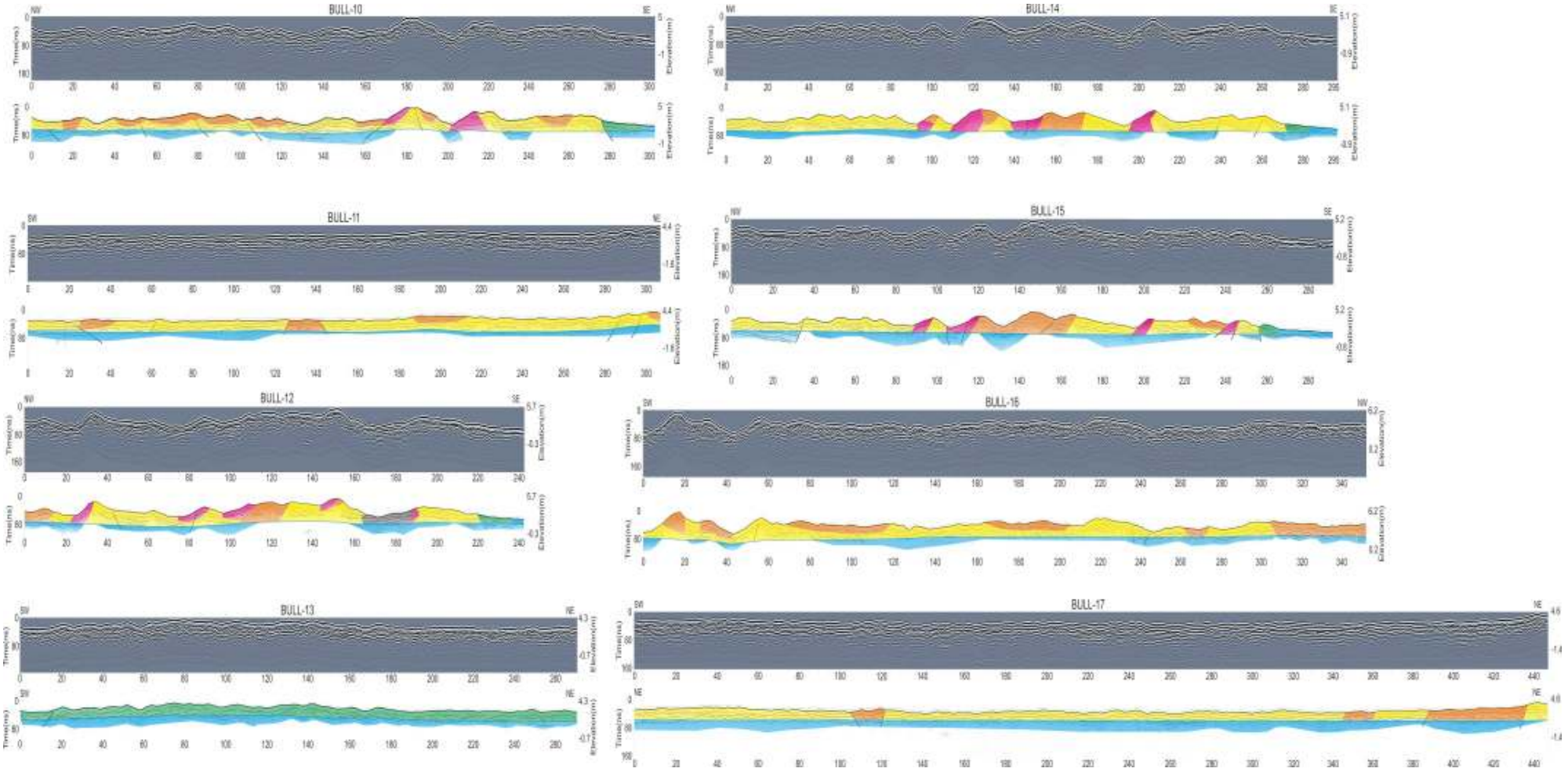

BULL ISLAND - SITE 3